Pedagogical Review of the Mølmer-Sørensen Gate in the Adiabatic Regime

David Verran

Abstract
This review presents a derivation and analysis of the core Mølmer-Sørensen (MS) gate dynamics in the regime of small Rabi frequencies and Lamb-Dicke factors, as well as symmetric detunings, Rabi frequency strengths, and phase. Under these assumptions, the Hamiltonian is derived from scratch, and a simple model for unitary evolution under it is derived using the Magnus expansion. Within this regime, we present an analysis of the key properties of the MS gate, and optimal tuning of the relevant experimental parameters for high fidelity is discussed. We extend this analysis further by presenting a crude derivation and analysis of the low-order dynamics obtained when pushing only slightly beyond the weak-driving regime, followed by a discussion of the major noise sources limiting the fidelity. We conclude with a construction of CNOT using the MS gate and single-qubit unitaries.

1 Introduction

Universal quantum computation requires the ability to construct both single-qubit and entangling 2-qubit unitaries with high fidelity [1][4]. For trapped-ion processors, one of the most promising gate designs for 2-qubit entangling gates is the Mølmer-Sørensen (hereafter MS) gate. This gate has the remarkable property that it is insensitive to the motional state of the ions, which allows it to operate at finite temperature [3][4].

Since the original conception of this gate in 1999 by Anders Sørensen and Klaus Mølmer [2], there have been a number of efforts to improve the design, in particular to speed up the gate time without sacrificing fidelity [7][10]. This is of critical importance as slow gate speeds are perhaps the most significant hindrance to the trapped-ion architecture when compared to competing modalities such as superconducting qubits [4]. Despite boasting longer coherence times, better connectivity of qubits and better prospects for scalability, gate speeds have historically been limited to the microsecond range, in stark contrast to the nanosecond speeds offered by superconducting qubits and competing modalities [4]. If fast high-fidelity 2-qubit gates can be realised experimentally, this author believes that this will solidify trapped-ion qubits as the superior modality for quantum computing. Whilst the subject of pulse shaping and other efforts to increase gate speed are beyond the scope of this review, we mention here the current direction of research in this gate and what it promises to deliver, to stress its relevance and importance to the field of quantum computing, in order to motivate a thorough understanding of the core dynamics of the gate as presented in the following.

2 Derivation of the Hamiltonian

We begin with a detailed derivation of the Hamiltonian for a simple toy model of an ion trap. The trap will contain 2 identical ions, each of which will have some electronic energy level structure. We adopt here the 2-level picture where we assume the remaining energy eigenstates of the ion's internal Hamiltonian will be sufficiently off-resonant from any lasers we will later add, such that they do not contribute to the dynamics of the system. In practice, these off-resonant states will typically induce

AC Stark shifts to the reduced 2-level system, but these will not be considered for the moment. The Hamiltonian of each ion will therefore be represented by some ground state $|g\rangle$ and some excited state $|e\rangle$ with energy $\hbar\omega_0$ above the ground state. These two states will form the computational basis states $|0\rangle$ and $|1\rangle$ for when we later use the trapped-ion system for quantum computation. This gives the following contribution to the Hamiltonian:

$$H_{electronic} = (|g\rangle\langle g| + \hbar\omega_0|e\rangle\langle e|) \otimes \mathbb{I} + \mathbb{I} \otimes (|g\rangle\langle g| + \hbar\omega_0|e\rangle\langle e|) \tag{1}$$

For simplicity, we will assume the two states $|g\rangle$ and $|e\rangle$ are dipole connected in this picture, although the same arguments will be applicable for higher order electric-quadrupole or magnetic-dipole connected states, or even for an effective Hamiltonian obtained from two-photon stimulated Raman transitions through some third virtual state.

When the ions are put into the trap, we must also allow for collective normal mode oscillations of the system. For 2 ions, there will be 2 modes (neglecting the transverse modes), but for the moment we assume that only one mode will be on-resonant whilst the other will not contribute to the dynamics. We therefore get a harmonic oscillator energy level structure at some trap frequency ν_0:

$$H_{motional} = \hbar\nu_0\hat{a}^\dagger\hat{a}, \tag{2}$$

where $\hat{a}^\dagger$ and $\hat{a}$ are the creation and annihilation operators for the motional phonon mode at frequency ν_0. Combining the two terms, we obtain the core Hamiltonian of the unperturbed system:

$$H_0 = H_{electronic} \otimes \mathbb{I}_{motional} + \mathbb{I}_{electronic} \otimes H_{motional} \tag{3}$$

The resulting energy level structure is shown in Figure 1:

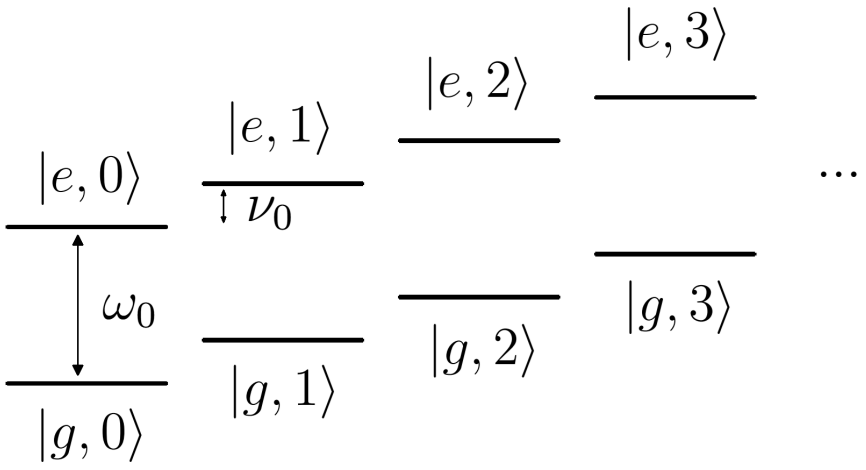

Figure 1: Energy level structure of H_0 in units of $\hbar$. The numbers denote the number of phonons in the motional subspace.

We now consider perturbing the ion trap system with 2 lasers. The lasers are for the moment assumed to be perfectly monochromatic at laser frequencies ω_{L1} and ω_{L2}. In the semi-classical picture, both ions will acquire dipole moments $-\hat{d}\cdot\vec{E}$. We therefore obtain a perturbation Hamiltonian:

$$
\begin{aligned}
H_{int} &= -\hat{d}_1 \cdot (\vec{E}_{L1}(z,t) + \vec{E}_{L2}(z,t)) \otimes \mathbb{I}_{ion2} \\
&\quad + \mathbb{I}_{ion1} \otimes -\hat{d}_2 \cdot (\vec{E}_{L1}(z,t) + \vec{E}_{L2}(z,t)) \\
&= \sum_{j=1}^{\#ions} \sum_{l=1}^{\#lasers} -\hat{d}_j \cdot \vec{E}_l(z,t)
\end{aligned} \tag{4}
$$

We take $\vec{E}_{L1} = E_0 \hat{x} \cos(k_{L1} z - \omega_{L1} t + \phi_{L1})$ and analogously for $\vec{E}_{L2}$. Note here we have implicitly assumed the two lasers have the same amplitude E_0 and thus their corresponding Rabi frequencies will be equivalent. Defining $\vec{r}_1$ to be the position of the valence electron of ion 1 relative to equilibrium and analogously for ion 2:

$$
\begin{aligned}
-\hat{d}_j \cdot \vec{E}_l &= e\vec{r}_j \cdot E_0 \hat{x} \cos(k_l z - \omega_l t + \phi_l) \\
&= \frac{e\hat{x}_j E_0}{2} (e^{i(k_l z - \omega_l t + \phi_l)} + e^{-i(k_l z - \omega_l t + \phi_l)})
\end{aligned} \tag{5}
$$

In the 2-level picture, we express the operator $\hat{x}$ in terms of the $\{|g\rangle, |e\rangle\}$ basis. For the dipole transitions considered here, selection rules will kill the diagonal elements via parity arguments, but we will find that similar arguments can be employed for the other cases (magnetic dipole, electric quadrupole, Raman) to yield:

$$
\begin{aligned}
\langle g|\hat{x}|g\rangle = \langle e|\hat{x}|e\rangle = 0 \\
\langle g|\hat{x}|e\rangle = \langle e|\hat{x}|g\rangle \in \mathbb{R} \text{ for bound states.}
\end{aligned} \tag{6}
$$

We therefore define the Rabi frequency Ω_R as follows:

$$
\hbar\Omega_R \equiv \langle g|e\hat{x}E_0|e\rangle, \tag{7}
$$

such that the operator $eE_0\hat{x}$ can be expressed as:

$$
\begin{aligned}
eE_0\hat{x} &= (|e\rangle\langle e| + |g\rangle\langle g|) eE_0\hat{x} (|e\rangle\langle e| + |g\rangle\langle g|) \\
&= \hbar\Omega_R (|e\rangle\langle g| + |g\rangle\langle e|) \\
&= \hbar\Omega_R \hat{\sigma}_x,
\end{aligned} \tag{8}
$$

where $\hat{\sigma}_x$ is the Pauli x operator. Substituting this back into the interaction Hamiltonian H_{int}:

$$
H_{int} = \sum_{j=1}^{\#ions} \sum_{l=1}^{\#lasers} \frac{\hbar\Omega_R}{2} (\hat{\sigma}_x^{(j)} e^{i(k_l z - \omega_l t + \phi_l)} + h.c.) \otimes \mathbb{I}_{motional}, \tag{9}
$$

where *h.c.* denotes the Hermitian conjugate. We now take the approximation that each ion is never displaced very far from equilibrium relative to the wavelengths of the driving lasers. By taking the operator $\hat{z}$ for each ion and recognising that we can represent this observable by $z_0(\hat{a} + \hat{a}^\dagger)$ (assuming that only this normal mode at frequency ν_0 is excited) for operators $\hat{a}$ and $\hat{a}^\dagger$ defined as above, we can formalise this assumption by taking the approximation that $kz_0 \ll 1$ for each laser mode k_{L1} and k_{L2}. This is the *Lamb-Dicke approximation*, and we can define the Lamb-Dicke factor $\eta \equiv kz_0$ to be

some small parameter which we assume is roughly equivalent for each ion. This equivalency will hold true for the centre-of-mass mode of oscillations, such that all ions vibrate equally [6]. This allows us to expand the exponential $e^{ikz} \approx 1 + ikz$ such that:

$$H_{int} = \sum_{j=1}^{\#ions} \sum_{l=1}^{\#lasers} \frac{\hbar\Omega_R}{2}(\hat{\sigma}_x^{(j)}(1 + i\eta(\hat{a} + \hat{a}^\dagger))e^{i(-\omega_l t+\phi_l)} + h.c.) \otimes \mathbb{I}_{motional} + O(\eta^2) \tag{10}$$

Lastly, it is common to move into an interaction picture rotating with the unperturbed Hamiltonian H_0. This picture is useful in order that the computational basis states and different phonon states do not acquire phase relative to each other over time. To transform into the interation frame, we make the mappings $\rho \to \tilde{\rho} \equiv \exp(\frac{iH_0t}{\hbar})\ \rho\ \exp(\frac{-iH_0t}{\hbar})$ and $H_{int} \to \tilde{H}_{int} \equiv \exp(\frac{iH_0t}{\hbar})\ H_{int}\ \exp(\frac{-iH_0t}{\hbar})$, where ρ is some density matrix evolving under the Hamiltonian $H_{tot} \equiv H_0 + H_{int}$. In this frame, the von Neumann equation $\frac{d}{dt}\rho = -\frac{i}{\hbar}[H_{tot}, \rho]$ can be shown to instead read $\frac{d}{dt}\tilde{\rho} = -\frac{i}{\hbar}[\tilde{H}_{int}, \tilde{\rho}]$, thus eliminating the phase accrual of the energy eigenstates of H_0. A proof of this claim is provided in Appendix A.1. We therefore require $\tilde{H}_{int}$:

$$\tilde{H}_{int} = \exp(\frac{iH_0t}{\hbar}) \sum_{j=1}^{\#ions} \sum_{l=1}^{\#lasers} \frac{\hbar\Omega_R}{2}(\hat{\sigma}_x^{(j)}(1 + i\eta(\hat{a} + \hat{a}^\dagger))e^{i(-\omega_l t+\phi_l)} + h.c.)\ \exp(\frac{-iH_0t}{\hbar}) \tag{11}$$

For atomic eigenstates $\{|g\rangle, |e\rangle\}$, $\hat{\sigma}_x$ only has non-zero matrix elements connecting $|g\rangle$ to $|e\rangle$ and vice versa. By considering explicly what happens in each case, we obtain:

$$\begin{aligned}
\langle g|e^{\frac{iH_0t}{\hbar}}\hat{\sigma}_x^{(j)}e^{\frac{-iH_0t}{\hbar}}|e\rangle &= \langle g|\hat{\sigma}_x^{(j)}e^{-i\omega_0 t}|e\rangle = e^{-i\omega_0 t} \\
\langle e|e^{\frac{iH_0t}{\hbar}}\hat{\sigma}_x^{(j)}e^{\frac{-iH_0t}{\hbar}}|g\rangle &= \langle e|e^{i\omega_0 t}\hat{\sigma}_x^{(j)}|g\rangle = e^{i\omega_0 t} \\
\implies e^{\frac{iH_0t}{\hbar}}\hat{\sigma}_x^{(j)}e^{\frac{-iH_0t}{\hbar}} &= e^{i\omega_0 t}\hat{\sigma}_+^{(j)} + e^{-i\omega_0 t}\hat{\sigma}_-^{(j)}
\end{aligned} \tag{12}$$

Similarly, for the motional space operators:

$$\begin{aligned}
\langle n|e^{\frac{iH_0t}{\hbar}}\hat{a}e^{\frac{-iH_0t}{\hbar}}|n+1\rangle &= \langle n|e^{n\nu_0 t}\hat{a}e^{-(n+1)\nu_0 t}|n+1\rangle \\
&= \langle n|\hat{a}|n+1\rangle e^{-\nu_0 t} \\
\langle n+1|e^{\frac{iH_0t}{\hbar}}\hat{a}^\dagger e^{\frac{-iH_0t}{\hbar}}|n\rangle &= \langle n+1|e^{(n+1)\nu_0 t}\hat{a}^\dagger e^{-n\nu_0 t}|n\rangle \\
&= \langle n+1|\hat{a}^\dagger|n\rangle e^{\nu_0 t} \\
\implies e^{\frac{iH_0t}{\hbar}}(\hat{a} + \hat{a}^\dagger)e^{\frac{-iH_0t}{\hbar}} &= \hat{a}e^{-\nu_0 t} + \hat{a}^\dagger e^{\nu_0 t}
\end{aligned} \tag{13}$$

Combining the above, we obtain for the interaction picture Hamiltonian:

$$\tilde{H}_{int} = \sum_{j=1}^{\#ions} \sum_{l=1}^{\#lasers} \frac{\hbar\Omega_R}{2}(e^{i\omega_0 t}\hat{\sigma}_+^{(j)} + e^{-i\omega_0 t}\hat{\sigma}_-^{(j)})(1 + i\eta(\hat{a}e^{-\nu_0 t} + \hat{a}^\dagger e^{\nu_0 t}))e^{i(-\omega_l t+\phi_l)} + h.c. \tag{14}$$

At this stage it becomes instructive for the purposes of quantum computing to reorganise the terms to explicitly show the particular transitions we may want to excite to construct various gates:

$$\begin{aligned}\tilde{H}_{int} &= \sum_{j=1}^{\#ions}\sum_{l=1}^{\#lasers}\frac{\hbar\Omega_R}{2}(e^{i\omega_0 t}\hat{\sigma}_+^{(j)} + e^{-i\omega_0 t}\hat{\sigma}_-^{(j)})e^{i(-\omega_l t+\phi_l)} + h.c. \\ &+ \frac{i\hbar\eta\Omega_R}{2}(e^{i\omega_0 t}\hat{\sigma}_+^{(j)} + e^{-i\omega_0 t}\hat{\sigma}_-^{(j)})(\hat{a}e^{-\nu_0 t} + \hat{a}^\dagger e^{\nu_0 t})e^{i(-\omega_l t+\phi_l)} + h.c. \\ &= \sum_{j=1}^{\#ions}\sum_{l=1}^{\#lasers}\frac{\hbar\Omega_R}{2}(e^{i\omega_0 t}\hat{\sigma}_+^{(j)} + e^{-i\omega_0 t}\hat{\sigma}_-^{(j)})e^{i(-\omega_l t+\phi_l)} + h.c. \\ &+ \frac{i\hbar\eta\Omega_R}{2}(e^{i(\omega_0-\nu_0)t}\hat{\sigma}_+^{(j)}\hat{a} + e^{-i(\omega_0-\nu_0)t}\hat{\sigma}_-^{(j)}\hat{a}^\dagger)e^{i(-\omega_l t+\phi_l)} + h.c. \\ &+ \frac{i\hbar\eta\Omega_R}{2}(e^{i(\omega_0+\nu_0)t}\hat{\sigma}_+^{(j)}\hat{a}^\dagger + e^{-i(\omega_0+\nu_0)t}\hat{\sigma}_-^{(j)}\hat{a})e^{i(-\omega_l t+\phi_l)} + h.c.\end{aligned} \tag{15}$$

Asserting now that the laser frequency detunings are chosen such that $\omega_l + \omega_0 \gg |\omega_l - \omega_0|$, where ω_0 gives the largest frequency scale in the system, we can make the rotating wave approximation (hereafter RWA) to kill off the far off-resonant terms:

$$\begin{aligned}\tilde{H}_{int} &= \sum_{j=1}^{\#ions}\sum_{l=1}^{\#lasers}\frac{\hbar\Omega_R}{2}e^{i((\omega_0-\omega_l)t+\phi_l)}\hat{\sigma}_+^{(j)} + h.c. \\ &+ \frac{i\hbar\eta\Omega_R}{2}e^{i((\omega_0-\nu_0-\omega_l)t+\phi_l)}\hat{\sigma}_+^{(j)}\hat{a} + h.c. \\ &+ \frac{i\hbar\eta\Omega_R}{2}e^{i((\omega_0+\nu_0-\omega_l)t+\phi_l)}\hat{\sigma}_+^{(j)}\hat{a}^\dagger + h.c.\end{aligned} \tag{16}$$

This form of the Hamiltonian is useful as it clearly separates the *carrier* and *sideband* transitions [3], which will be defined in the following. The first term of strength $\frac{\hbar\Omega_R}{2}$ and with only the $\hat{\sigma}_+$ and $\hat{\sigma}_-$ operators gives the *carrier* transition, which allows for transitions between the computational $|g\rangle$ and $|e\rangle$ states without changing the phonon subspace. The next two terms are the *sideband* terms, and are weaker by a factor of η, which we remind here is chosen to be small such that the previously made Lamb-Dicke approximation is valid. The first sideband term is the *red* sideband transition and induces transitions between $|g, n\rangle$ and $|e, n-1\rangle$ states, where n denotes some number of phonons. The second sideband term is the *blue* sideband transition, and induces transitions between $|g, n\rangle$ and $|e, n+1\rangle$ states. These transitions are shown in Figure 2:

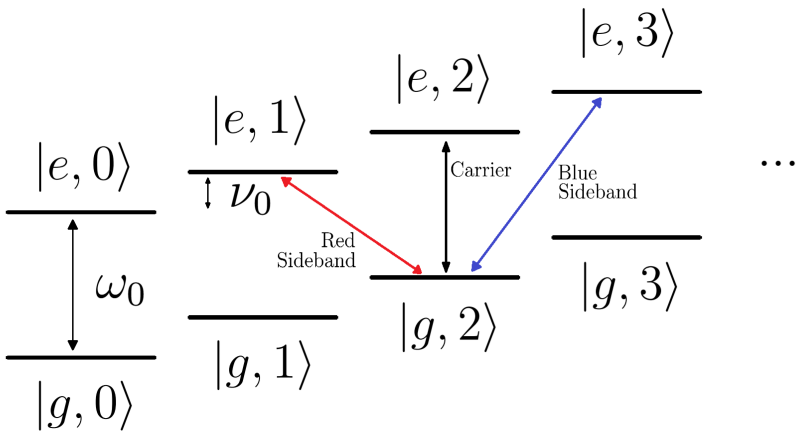

Figure 2: Carrier transition and the red and blue sideband transitions.

3 Derivation of the Gate Dynamics

In this section we derive the evolution operator for the Hamiltonian derived in Section 2 for the particular choice of laser frequencies and detunings as used in the MS gate. For the simplest toy model of the MS gate as worked through in the following, we fix the number of ions and the number of laser frequencies to 2. The goal is to obtain the following entangling gate:

$$U_{MS} = \frac{1}{\sqrt{2}} \begin{pmatrix} 1 & 0 & 0 & -i \\ 0 & 1 & -i & 0 \\ 0 & -i & 1 & 0 \\ -i & 0 & 0 & 1 \end{pmatrix}, \tag{17}$$

which we will later show is equivalent to a controlled phase C-Z gate (up to global single-qubit rotations).

Practically, this gate will be constructed by first achieving Rabi oscillations between the states $|gg\rangle$ and $|ee\rangle$, and between the states $|ge\rangle$ and $|eg\rangle$, then choosing the gate time such that we prematurely terminate the oscillation half-way. In this way, $|gg\rangle$ does not fully reach $|ee\rangle$, but we instead achieve the entangled state $\frac{1}{\sqrt{2}}(|gg\rangle - i|ee\rangle)$.

To construct Rabi oscillations in this way, the laser detunings are chosen such that we drive Raman transitions through the sidebands by only virtually exciting different phonon modes. In the simplest implementation of the MS gate, the laser frequencies $\omega_{L1} = \omega_0 - \nu_0 - \delta$ and $\omega_{L2} = \omega_0 + \nu_0 + \delta$ are chosen, where δ is a small detuning from the sidebands. Figure 3 shows how these detunings ensure that only the required transitions described above are Raman on-resonant:

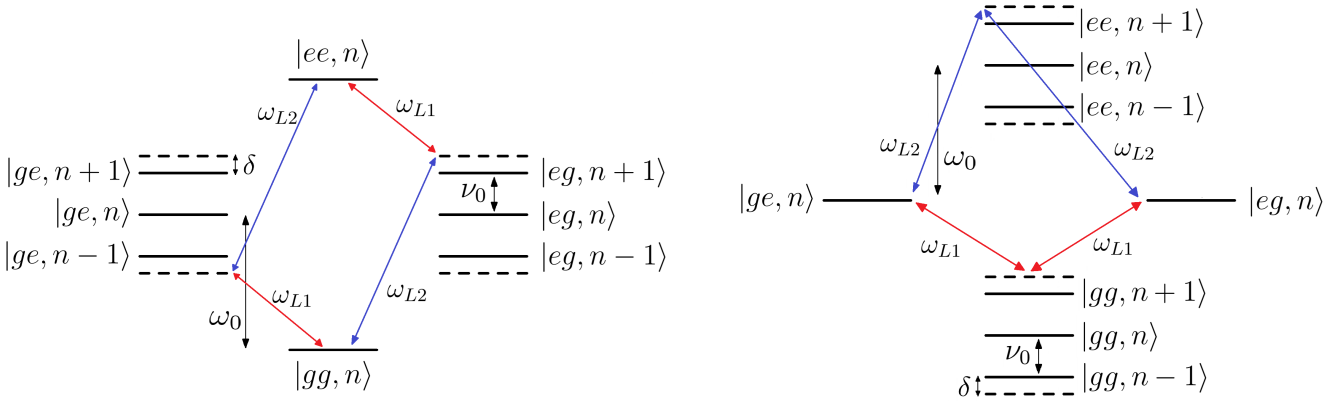

Figure 3: Raman transitions for MS gate. $|gg\rangle \longleftrightarrow |ee\rangle$ (left) and $|ge\rangle \longleftrightarrow |eg\rangle$ (right).

Substituting these values for ω_{L1} and ω_{L2} into the Hamiltonian derived in Section 2, and additionally taking symmetric phases $\phi_{L1} = \phi_{L2} = \phi$, we obtain:

$$\begin{aligned} \tilde{H}_{int} = \sum_{j=1}^{\#ions} & \frac{\hbar\Omega_R}{2}(e^{i((\nu_0+\delta)t+\phi)} + e^{i((-\nu_0-\delta)t+\phi)})\hat{\sigma}_+^{(j)} + h.c. \\ & + \frac{i\hbar\eta\Omega_R}{2}(e^{i(\delta t+\phi)} + e^{i((-2\nu_0-\delta)t+\phi)})\hat{\sigma}_+^{(j)}\hat{a} + h.c. \\ & + \frac{i\hbar\eta\Omega_R}{2}(e^{i((2\nu_0+\delta)t+\phi)} + e^{i(-\delta t+\phi)})\hat{\sigma}_+^{(j)}\hat{a}^\dagger + h.c. \end{aligned} \tag{18}$$

At this point, a second RWA can be made to drop the fast oscillation terms. We will lose the carrier transition entirely, and keep only the red and blue sideband terms oscillating with frequency δ. This approximation will not necessarily be valid beyond the weak-driving regime, where Rabi frequencies are chosen to be larger in order to achieve faster gates. This is because although the carrier terms are off-resonant, they are larger by a factor of $\frac{1}{\eta}$ relative to the sidebands, and thus for sufficiently large Rabi frequencies relative to the detuning from the carrier $\nu_0 + \delta$, we will not be able to completely disregard its effects. We will discuss this regime further in Section 5. Nevertheless, for the simple setup we derive here, the second RWA is assumed to be valid for sufficiently large detunings $\nu_0 + \delta$. This yields the Hamiltonian:

$$\tilde{H}_{int} = \sum_{j=1}^{\#ions} \frac{i\hbar\eta\Omega_R e^{i\phi}}{2} \hat{\sigma}_+^{(j)} (e^{i\delta t}\hat{a} + e^{-i\delta t}\hat{a}^\dagger) + h.c. \tag{19}$$

For notational convenience, it is often useful to re-express $\hat{S}_+ \equiv \sum_{j=1}^{\#ions} \hat{\sigma}_+^{(j)}$, and additionally, to absorb the phase ϕ into $\hat{S}_+$ such that we can define $\hat{S}_+^{(\phi)} \equiv \hat{S}_+ e^{i\phi}$. Substituting into (19), we obtain:

$$\tilde{H}_{int} = \frac{i\hbar\eta\Omega_R}{2} \hat{S}_+^{(\phi)} (e^{i\delta t}\hat{a} + e^{-i\delta t}\hat{a}^\dagger) + h.c. \tag{20}$$

Lastly, by noting that $i\hat{\sigma}_+ + h.c. = -\hat{\sigma}_y$, we can analogously define $-\hat{S}_y^{(\phi)} \equiv i\hat{S}_+^{(\phi)} + h.c.$, which allows us to later exploit properties of Pauli matrices to ease calculations. Crucially, we find that $\hat{\sigma}_y^{(\phi)}$ will share similar properties to the standard $\hat{\sigma}_y$ operator, most notably:

$$\begin{aligned} \hat{\sigma}_y^{(\phi)2} &\equiv (-i\hat{\sigma}_+^{(\phi)} + i\hat{\sigma}_-^{(\phi)})^2 \\ &= (-i\hat{\sigma}_+ e^{i\phi} + i\hat{\sigma}_- e^{-i\phi})^2 \\ &= \hat{\sigma}_+\hat{\sigma}_- e^{i(\phi-\phi)} + \hat{\sigma}_-\hat{\sigma}_+ e^{i(-\phi+\phi)} \\ &= \mathbb{I}. \end{aligned} \tag{21}$$

This final substitution yields our final form for the simplified MS Hamiltonian:

$$\tilde{H}_{int} = -\frac{\hbar\eta\Omega_R}{2} \hat{S}_y^{(\phi)} (e^{i\delta t}\hat{a} + e^{-i\delta t}\hat{a}^\dagger) \tag{22}$$

We are now ready to derive the form of the evolution operator.

3.1 Derivation of MS Evolution Operator

In the following we solve for the evolution operator $U(t)$, defined by the time-evolution equation:

$$|\Psi(t)\rangle = U(t)|\Psi(t_0)\rangle \tag{23}$$

The evolution operator can be obtained from the Schrodinger equation:

$$i\hbar\frac{\partial}{\partial t}U(t) = H(t)U(t) \tag{24}$$

Unfortunately, the form of the Hamiltonian $\tilde{H}_{int}(t)$ for the trapped-ion system makes direct integration of this equation to find a solution for $U(t)$ impossible. This is because the commutator $[\tilde{H}(t_1), \tilde{H}(t_2)]$ for two different times t_1 and t_2 does not vanish in general, thus simply exponentiating the integral of $\tilde{H}(t)$ does not work in this case.

One possible solution is to instead use the *Magnus expansion*, where we assume a solution exists for the evolution operator $U(t)$ of the form $\exp(\Omega(t))$, where $\Omega(t)$ is found from a series expansion:

$$\Omega(t) = \Omega_1(t) + \Omega_2(t) + \Omega_3(t) + \dots \tag{25}$$

This expansion is useful as any premature truncation at finite order will still yield a unitary approximation due to the exponential structure, which in general will not be true for alternative methods such as the Dyson Series. A more in-depth discussion of the Magnus expansion including convergence properties can be found in [8].

The first few terms of the Magnus expansion are given by:

$$\begin{aligned}
\Omega_1(t) &= -\frac{i}{\hbar}\int_{t_0}^{t} dt_1 H(t_1) \\
\Omega_2(t) &= -\frac{1}{2\hbar^2}\int_{t_0}^{t} dt_1 \int_{t_0}^{t_1} dt_2 [H(t_1), H(t_2)] \\
\Omega_3(t) &= \frac{i}{6\hbar^3}\int_{t_0}^{t} dt_1 \int_{t_0}^{t_1} dt_2 \int_{t_0}^{t_2} dt_3 ([H(t_1), [H(t_2), H(t_3)]] + [H(t_3), [H(t_2), H(t_1)]])
\end{aligned} \tag{26}$$

We apply this to the MS Hamiltonian (22):

$$\begin{aligned}
\Omega_1(t) &= -\frac{i}{\hbar}\int_{0}^{t} dt_1 \tilde{H}(t_1) \\
&= \frac{i}{\hbar}\int_{0}^{t} dt_1 \frac{\hbar\eta\Omega_R}{2}\hat{S}_y^{(\phi)}(e^{i\delta t_1}\hat{a} + e^{-i\delta t_1}\hat{a}^\dagger) \\
&= \frac{i\eta\Omega_R}{2}\hat{S}_y^{(\phi)}(\frac{1}{i\delta}(e^{i\delta t} - 1)\hat{a} - \frac{1}{i\delta}(e^{-i\delta t} - 1)\hat{a}^\dagger) \\
&= \frac{\eta\Omega_R}{2\delta}\hat{S}_y^{(\phi)}((e^{i\delta t} - 1)\hat{a} - (e^{-i\delta t} - 1)\hat{a}^\dagger)
\end{aligned} \tag{27}$$

In order to obtain $\Omega_2(t)$, it is first necessary to find an expression for the commutator of $\tilde{H}_{int}(t)$ with itself at different times:

$$\begin{aligned}
[\tilde{H}_{int}(t_1), \tilde{H}_{int}(t_2)] &= [-\frac{\hbar\eta\Omega_R}{2}\hat{S}_y^{(\phi)}(e^{i\delta t_1}\hat{a} + e^{-i\delta t_1}\hat{a}^\dagger), -\frac{\hbar\eta\Omega_R}{2}\hat{S}_y^{(\phi)}(e^{i\delta t_2}\hat{a} + e^{-i\delta t_2}\hat{a}^\dagger)] \\
&= (\frac{\hbar\eta\Omega_R}{2})^2\hat{S}_y^{(\phi)2}(e^{i\delta(t_1-t_2)}[\hat{a}, \hat{a}^\dagger] + e^{-i\delta(t_1-t_2)}[\hat{a}^\dagger, \hat{a}]) \\
&= (\frac{\hbar\eta\Omega_R}{2})^2\hat{S}_y^{(\phi)2}(e^{i\delta(t_1-t_2)} - e^{-i\delta(t_1-t_2)}) \otimes \mathbb{I}_{motional} \\
&= (\frac{\hbar\eta\Omega_R}{2})^2\hat{S}_y^{(\phi)2} \cdot 2i\sin(\delta(t_1 - t_2))
\end{aligned} \tag{28}$$

Substituting this into the second Magnus expansion term $\Omega_2(t)$:

$$\begin{aligned}
\Omega_2(t) &= -\frac{1}{2\hbar^2}\int_{t_0}^{t} dt_1 \int_{t_0}^{t_1} dt_2 [H(t_1), H(t_2)] \\
&= -\frac{1}{2\hbar^2}\int_{0}^{t} dt_1 \int_{t_0}^{t_1} dt_2 (\frac{\hbar\eta\Omega_R}{2})^2 \hat{S}_y^{(\phi)2} \cdot 2i\sin(\delta(t_1 - t_2)) \\
&= -i(\frac{\eta\Omega_R}{2})^2 \hat{S}_y^{(\phi)2} \int_{t_0}^{t} dt_1 \frac{1}{\delta}(1 - \cos(\delta t_1)) \\
&= -i(\frac{\eta\Omega_R}{2\delta})^2 \hat{S}_y^{(\phi)2}(\delta t - \sin(\delta t))
\end{aligned} \tag{29}$$

Remarkably, as the commutator of $\tilde{H}_{int}(t)$ with itself at different times goes like $\hat{S}_y^{(\phi)2} \otimes \mathbb{I}_{motional}$, we obtain that $[\tilde{H}_{int}(t_1), [\tilde{H}_{int}(t_2), \tilde{H}_{int}(t_3)]] = 0$, and by extension all higher order commutators will also conveniently vanish. Thus, the Magnus expansion to only second order will give us an exact evolution operator for $\tilde{H}_{int}(t)$. Note however, it is worth stating again that this does not mean we have solved for the exact MS gate dynamics, as the Hamiltonian used here was obtained after 2 rotating wave approximations, the second of which may not necessarily be valid. Further, noise effects including (but not limited to) spontaneous emission, stray magnetic fields, heating, as well as other off-resonant states of the ions have not been accounted for (we will discuss these in more detail in Section 6). Nevertheless, within the regime of well-isolated, long coherence time trapped-ions well within the Lamb-Dicke regime and with small Rabi frequencies, these two terms are sufficient to give an accurate representation of the gate dynamics we should expect. The final step is to combine them and obtain the evolution operator $U(t)$:

$$\begin{aligned}
U(t) &= \exp(\Omega_1(t) + \Omega_2(t)) \\
&= \exp(\Omega_1(t)) \cdot \exp(\Omega_2(t)) \text{ (as } \Omega_1(t) \text{ and } \Omega_2(t) \text{ commute)} \\
&= \exp(\frac{\eta\Omega_R}{2\delta}\hat{S}_y^{(\phi)}((e^{i\delta t} - 1)\hat{a} - (e^{-i\delta t} - 1)\hat{a}^\dagger)) \cdot \exp(-i(\frac{\eta\Omega_R}{2\delta})^2 \hat{S}_y^{(\phi)2}(\delta t - \sin(\delta t)))
\end{aligned} \tag{30}$$

3.2 Obtaining the MS gate unitary

We will now choose parameters δ and Ω_R such that at the gate time t_g, we obtain the MS gate unitary given in (17). The first term in (30) given by $\exp(\Omega_1(t))$ is typically referred to as the *displacement operator* [7], and is responsible for the motion of the phonon states in phase space. This motion is unwanted for the entangling MS gate we want to obtain, so we will want to eliminate its contribution. By inspection, we immediately see that taking $\delta t = 2\pi m$ for $m \in \mathbb{Z}$ will cause $\exp(\Omega_1(t))$ to just give the identity. Additionally, this causes the second term to lose the contribution from $\sin(\delta t)$, as this will equal zero. The process of choosing the detuning in this way, such that δt is an integer multiple of 2π, is called the *loop closure* condition, as it is equivalent to ensuring that all phonon trajectories in phase space form closed loops and return to their original state at the gate time. By consequence, the MS gate will be insensitive to the motional state of the input [3][4], which gives it the useful property that it will still work at finite temperature. Enforcing this condition at the gate time t_g, we obtain a much simpler form for the evolution operator:

$$U(t_g) = \exp(-i\delta t_g(\frac{\eta\Omega_R}{2\delta})^2 \hat{S}_y^{(\phi)2}) \tag{31}$$

To exponentiate this matrix, we note that $\hat{S}_y^{(\phi)2}$ has the following useful property:

$$\begin{aligned}\hat{S}_y^{(\phi)2} &= (\hat{\sigma}_y^{(\phi)} \otimes \mathbb{I} + \mathbb{I} \otimes \hat{\sigma}_y^{(\phi)})^2 \\ &= (\hat{\sigma}_y^{(\phi)2} \otimes \mathbb{I}^2 + 2\hat{\sigma}_y^{(\phi)} \otimes \hat{\sigma}_y^{(\phi)} + \mathbb{I}^2 \otimes \hat{\sigma}_y^{(\phi)2}) \\ &= 2(\mathbb{I} \otimes \mathbb{I} + \hat{\sigma}_y^{(\phi)} \otimes \hat{\sigma}_y^{(\phi)})\end{aligned} \tag{32}$$

$$\begin{aligned}(\hat{S}_y^{(\phi)2})^2 &= 4(\mathbb{I}^2 \otimes \mathbb{I}^2 + 2\hat{\sigma}_y^{(\phi)} \otimes \hat{\sigma}_y^{(\phi)} + \hat{\sigma}_y^{(\phi)2} \otimes \hat{\sigma}_y^{(\phi)2}) \\ &= 4 \cdot 2(\mathbb{I} \otimes \mathbb{I} + \hat{\sigma}_y^{(\phi)} \otimes \hat{\sigma}_y^{(\phi)}) \\ &= 4\hat{S}_y^{(\phi)2}\end{aligned} \tag{33}$$

And thus,

$$(\frac{1}{4}\hat{S}_y^{(\phi)2})^n = \frac{1}{4}\hat{S}_y^{(\phi)2} \quad \forall\ n \in \mathbb{Z} \tag{34}$$

This allows us to express the exponential in a more convenient form:

$$\begin{aligned}U(t_g) &= \exp(-i\delta t_g(\frac{\eta\Omega_R}{2\delta})^2 \hat{S}_y^{(\phi)2}) \\ &= \exp(-it_g\frac{\eta^2\Omega_R^2}{\delta}\frac{1}{4}\hat{S}_y^{(\phi)2}) \\ &= \mathbb{I} + (-it_g\frac{\eta^2\Omega_R^2}{\delta})(\frac{1}{4}\hat{S}_y^{(\phi)2}) + \frac{1}{2}(-it_g\frac{\eta^2\Omega_R^2}{\delta})^2(\frac{1}{4}\hat{S}_y^{(\phi)2})^2 + \dots \\ &= \mathbb{I} - (\frac{1}{4}\hat{S}_y^{(\phi)2}) + (\frac{1}{4}\hat{S}_y^{(\phi)2})(\mathbb{I} + (-it_g\frac{\eta^2\Omega_R^2}{\delta}) + \frac{1}{2}(-it_g\frac{\eta^2\Omega_R^2}{\delta})^2 + \dots) \\ &= \mathbb{I} - (\frac{1}{4}\hat{S}_y^{(\phi)2}) + \exp(-it_g\frac{\eta^2\Omega_R^2}{\delta})(\frac{1}{4}\hat{S}_y^{(\phi)2})\end{aligned} \tag{35}$$

At this point it becomes convenient to define the effective Rabi frequency for the MS gate oscillations $\Omega \equiv \frac{\eta^2\Omega_R^2}{2\delta}$. To obtain the final form of the MS gate, we re-express (35) in matrix form for ease of manipulation. For this, we require the matrix representing $\hat{S}_y^{(\phi)2}$:

$$\begin{aligned}\hat{S}_y^{(\phi)2} &= 2(\mathbb{I} \otimes \mathbb{I} + \hat{\sigma}_y^{(\phi)} \otimes \hat{\sigma}_y^{(\phi)}) \text{ (from (32))} \\ &= 2(\mathbb{I} \otimes \mathbb{I} + \begin{pmatrix} 0 & -ie^{i\phi} \\ ie^{-i\phi} & 0 \end{pmatrix} \otimes \begin{pmatrix} 0 & -ie^{i\phi} \\ ie^{-i\phi} & 0 \end{pmatrix}) \\ &= 2\begin{pmatrix} 1 & 0 & 0 & 0 \\ 0 & 1 & 0 & 0 \\ 0 & 0 & 1 & 0 \\ 0 & 0 & 0 & 1 \end{pmatrix} + 2\begin{pmatrix} 0 & 0 & 0 & -e^{2i\phi} \\ 0 & 0 & 1 & 0 \\ 0 & 1 & 0 & 0 \\ -e^{-2i\phi} & 0 & 0 & 0 \end{pmatrix} \\ &= 2\begin{pmatrix} 1 & 0 & 0 & -e^{2i\phi} \\ 0 & 1 & 1 & 0 \\ 0 & 1 & 1 & 0 \\ -e^{-2i\phi} & 0 & 0 & 1 \end{pmatrix}\end{aligned} \tag{36}$$

Substituting this expression into $U(t_g)$, we obtain:

$$
\begin{aligned}
U(t_g) &= \begin{pmatrix} 1 & 0 & 0 & 0 \\ 0 & 1 & 0 & 0 \\ 0 & 0 & 1 & 0 \\ 0 & 0 & 0 & 1 \end{pmatrix} - \frac{1}{2}\begin{pmatrix} 1 & 0 & 0 & -e^{2i\phi} \\ 0 & 1 & 1 & 0 \\ 0 & 1 & 1 & 0 \\ -e^{-2i\phi} & 0 & 0 & 1 \end{pmatrix} + \frac{1}{2}\begin{pmatrix} 1 & 0 & 0 & -e^{2i\phi} \\ 0 & 1 & 1 & 0 \\ 0 & 1 & 1 & 0 \\ -e^{-2i\phi} & 0 & 0 & 1 \end{pmatrix} e^{-2i\Omega t_g} \\
&= \frac{1}{2}\begin{pmatrix} 1+e^{-2i\Omega t_g} & 0 & 0 & e^{2i\phi}(1-e^{-2i\Omega t_g}) \\ 0 & 1+e^{-2i\Omega t_g} & e^{-2i\Omega t_g}-1 & 0 \\ 0 & e^{-2i\Omega t_g}-1 & 1+e^{-2i\Omega t_g} & 0 \\ e^{-2i\phi}(1-e^{-2i\Omega t_g}) & 0 & 0 & 1+e^{-2i\Omega t_g} \end{pmatrix} \\
&= e^{-i\Omega t_g}\begin{pmatrix} \cos(\Omega t_g) & 0 & 0 & ie^{2i\phi}\sin(\Omega t_g) \\ 0 & \cos(\Omega t_g) & -i\sin(\Omega t_g) & 0 \\ 0 & -i\sin(\Omega t_g) & \cos(\Omega t_g) & 0 \\ ie^{-2i\phi}\sin(\Omega t_g) & 0 & 0 & \cos(\Omega t_g) \end{pmatrix}
\end{aligned} \tag{37}
$$

To achieve only half-way Rabi oscillations, we take $\Omega t_g = \frac{\pi}{4}$:

$$
U(t_g) = \frac{1}{\sqrt{2}}\begin{pmatrix} 1 & 0 & 0 & ie^{2i\phi} \\ 0 & 1 & -i & 0 \\ 0 & -i & 1 & 0 \\ ie^{-2i\phi} & 0 & 0 & 1 \end{pmatrix}, \tag{38}
$$

up to a global phase. For a choice of $\phi = \frac{\pi}{2}$, we obtain the entangling MS gate unitary presented in (17).

4 Optimising Parameters

The derivation in Section 3 enforces a number of conditions on the parameters involved in order that our gate achieves the required mappings at high fidelity. This section discusses how these conditions can be satisfied simultaneously, and examines the impacts of deviations from their optimal values. As at this stage we begin to discuss the optimisation of real experimental parameters, we will instantiate our toy model with a particular choice of physical implementation of trapped-ion qubits later in this section, in order to obtain values for realistic gate times and to justify any approximations we have thus far made.

We list here the requirements derived above (not a comprehensive list) that need to be fulfilled:

- We require $\eta\sqrt{n} \ll 1$ in order that we are in the Lamb-Dicke regime and can disregard terms of order η^2.
- We require that $\frac{\Omega_R}{\delta+\nu_0} \ll 1$ such that we remain in the weak-driving regime and can justify applying the second RWA to the carrier transitions. This condition and its violation will be discussed in more detail in Section 5.
- We require symmetric detunings δ from the two sideband transitions, as well as equal Rabi frequency strengths between the two laser frequencies. This is necessary to prevent any AC Stark shifts that will alter the phase accrual of the logical states.
- We require that the phases of the lasers be equivalent. For the particular choice of entangling gate we derived in Section 3, we additionally take $\phi = \frac{\pi}{2}$ to achieve the mappings $|gg\rangle \rightarrow \frac{1}{\sqrt{2}}(|gg\rangle - i|ee\rangle)$ and analogously for $|ee\rangle$. Note the mappings of $|ge\rangle$ and $|eg\rangle$ are insensitive to the particular choice of ϕ, assuming they are the same for both lasers.

- We require that the loop closure condition $\delta t_g = 2\pi m$ for $m \in \mathbb{Z}$ be fulfilled, such that the gate is insensitive to the motional state of the ions.
- Lastly, we require that the gate time t_g is chosen such that the Rabi oscillations at frequency $\Omega \equiv \frac{\Omega_R^2 \eta^2}{2\delta}$ are stopped half-way on the trajectory around the Bloch sphere from $|gg\rangle$ to $|ee\rangle$, and analogously for the other 3 2-qubit logical states.

It is worth stating that the conditions derived above may be violated intentionally when going beyond the weak-driving regime in the interests of counteracting additional errors that may arise here. For example, it is common to deliberately choose imbalances in the individual laser Rabi frequencies to create AC Stark shifts, which can be used to cancel other experimental sources of AC Stark shifts due to off-resonant scattering [6][11].

Interestingly, as stated above in Section 3, we find that following the loop closure condition, there will be no explicit requirement on the motional phonon state. In addition to allowing for any number of phonons (provided we remain in the Lamb-Dicke regime), this insensitivity is more powerful in that we also allow for any general superposition state of different numbers of phonons. This is one of the most appealing properties of the MS gate architecture, and one that makes it superior to its predecessor, the Cirac-Zoller gate, which only works correctly when the system is cooled to having exactly zero phonons [3].

The final two conditions discussing the loop closure condition and the gate timing can be combined to give the following requirement on δ:

$$\begin{aligned} 2\pi \frac{\delta^2}{\Omega_R^2 \eta^2} &= 2\pi m \\ \implies \delta &= 2\Omega_R \eta \sqrt{m} \end{aligned} \tag{39}$$

Common choices of m are typically small integers in the range of 1-4, which is motivated by keeping δ as small as possible [2]. As the effective Rabi frequency for the MS gate oscillations scales like $\sim \frac{1}{\delta}$, smaller detunings are motivated largely by a desire to construct faster gates. Further, for larger δ, it becomes experimentally harder to set the gate time t_g exactly to satisfy loop closure, as small offsets in timings could result in a large phase δt.

Figures 4 and 5 show plots of the Rabi oscillations obtained for the transition between $|gg\rangle$ and $|ee\rangle$ with and without the loop closure condition being satisfied respectively. We find, as expected, that the fidelities obtained with loop closure are much higher than those obtained without. The model parameters are taken from the setup described in [11], where the qubit is taken to be two quadrupole-connected levels of the $^{40}Ca^+$ ion. The energy splitting $\hbar\omega_0$ for these states is in the optical range with wavelength 729nm, thus qubits such as these are referred to as 'optical qubits'. The setup in [11] uses a linear Paul trap operating such that the axial centre-of-mass mode will have frequency $\nu_0 = 1$MHz, and the global beam for MS gate operation has Lamb-Dicke factor $\eta = 0.06$.

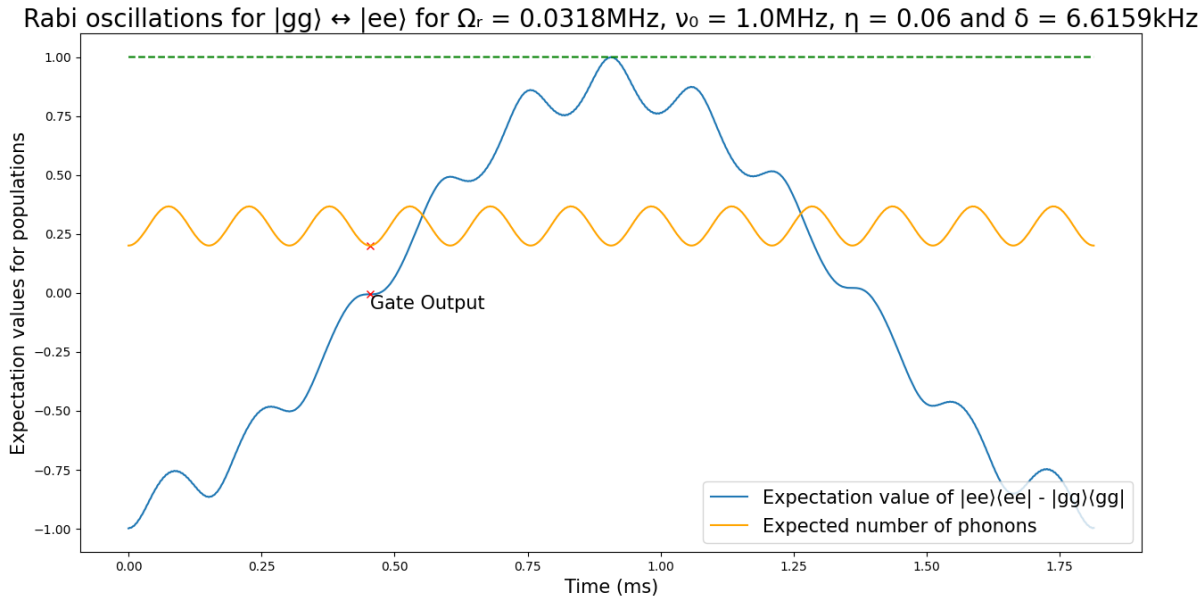

Figure 4: Rabi oscillations for $|gg\rangle \leftrightarrow |ee\rangle$ transitions for one cycle. The detuning δ is given by (39) with a choice of $m = 3$. This plot was produced for the parameters given in the graph title using a numerical Lindblad master equation solver in QuTip. The whole simulation can be found on my GitHub page under the name of MS gate.py. The orange line gives phonon oscillations governed by the displacement operator, with an initial motional state given by a thermal density matrix with an average number of phonons of 0.2. We note that at the gate time (red x), the oscillations return to its original value, as required. Without applying any rotating wave approximations and just using the raw Hamiltonian as given by (15), we obtain a fidelity for this mapping of $|gg\rangle \rightarrow \frac{1}{\sqrt{2}}(|gg\rangle - i|ee\rangle)$ of 0.99991.

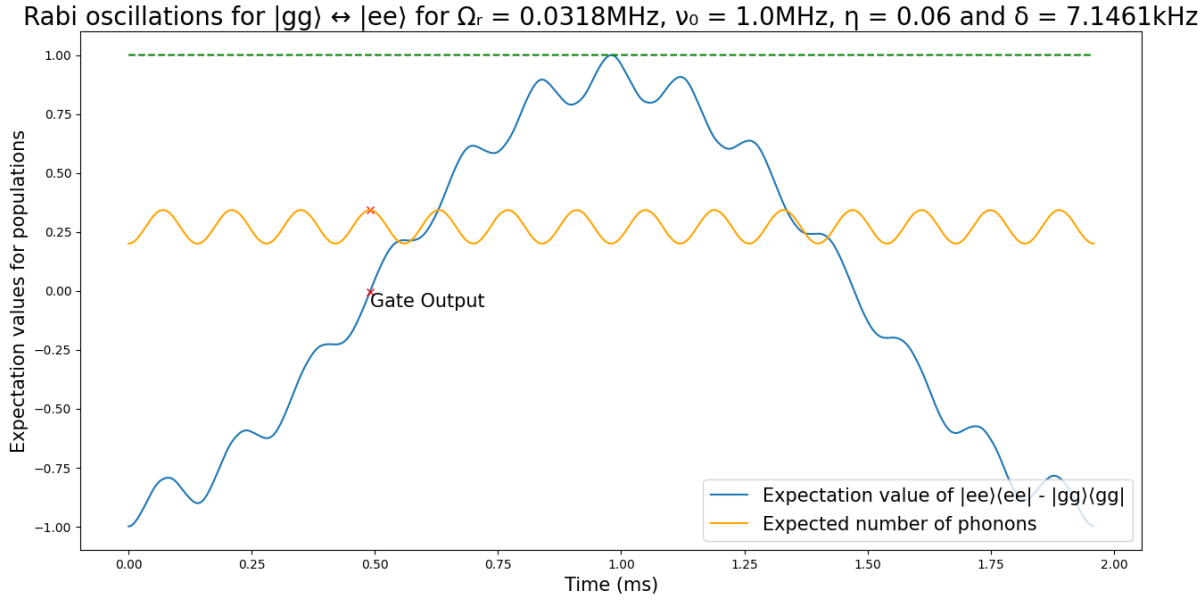

Figure 5: The same setup as in Figure 4, but with a non-integer choice of $m = 3.5$. Taking half-integer values of m like this will maximally violate the loop closure condition. The resulting fidelity for this mapping is therefore significantly lower than before, at 0.9161.

5 Impact of Carrier Transition

This section provides a rough, non-rigorous overview of the low-order impacts of the carrier transition in limiting the MS gate fidelity. Modelling the gate effectively in the presence of these off-resonant effects is far from trivial, as the most straightforward approach of calculating a complete Magnus expansion becomes far more cumbersome to calculate at low order, and near intractable at higher orders. Thus, the approach demonstrated here serves only to give insight into the dominant effects of the carrier transition, and disregards higher order terms that can be safely neglected when we only slightly push beyond the weak-driving regime.

Firstly, to motivate why it becomes necessary to consider the carrier transition at all, we consider what happens when we attempt to speed up the gate. This is of critical importance, as slow gate speeds are one of the most pressing challenges faced by trapped-ion quantum computing. Although this modality boasts unrivaled coherence times and record fidelities, when comparing to competing modalities such as superconducting qubits, the gate speeds for 2-qubit entangling unitaries are typically several orders of magnitude lower [4].

To decrease the gate time, the most obvious approach would be to increase the effective Rabi frequency $\frac{\Omega_R^2\eta^2}{2\delta}$, which experimentally is typically achieved by increasing Ω_R. The Lamb-Dicke factor η is less experimentally accessible as a variable parameter, and the detuning δ was formerly shown to be proportional to Ω_R by consequence of loop closure. Thus, the solution would be to increase Ω_R, which is typically achieved by increasing the laser amplitude E_0.

In the following we will show that increasing Ω_R relative to the carrier detuning $\nu_0+\delta$ will increase the effects of the carrier transition, thus forcing us to consider its effects when constructing faster gates. The procedure we use here is *adiabatic elimination*, where we start from the complete Schrodinger equation involving all relevant states and couplings, then assuming that some probability amplitudes will evolve much faster than others, we can *adiabatically eliminate* the off-resonant states and obtain an effective system of equations for the dynamics of the resulting two-level system. Although this is a less rigorous method than the Dyson series or Magnus expansion, it is far simpler to calculate and still recovers the core features of the carrier effects at low order.

5.1 Adiabatic Elimination of Carrier Transition Levels

We begin by restating (18) here to give the form of the Hamiltonian for the trapped-ion system prior to making the second RWA:

$$\begin{aligned}\tilde{H}_{int} = &\sum_{j=1}^{\#ions} \frac{\hbar\Omega_R}{2}(e^{i((\nu_0+\delta)t+\phi)} + e^{i((-\nu_0-\delta)t+\phi)})\hat{\sigma}_+^{(j)} + h.c. \\ &+ \frac{i\hbar\eta\Omega_R}{2}(e^{i(\delta t+\phi)} + e^{i((-2\nu_0-\delta)t+\phi)})\hat{\sigma}_+^{(j)}\hat{a} + h.c. \\ &+ \frac{i\hbar\eta\Omega_R}{2}(e^{i((2\nu_0+\delta)t+\phi)} + e^{i(-\delta t+\phi)})\hat{\sigma}_+^{(j)}\hat{a}^\dagger + h.c. \\ = &\frac{\hbar\Omega_R}{2}\hat{S}_+(e^{i((\nu_0+\delta)t+\phi)} + e^{i((-\nu_0-\delta)t+\phi)}) + h.c. + \text{ sideband terms.}\end{aligned} \tag{40}$$

We immediately take $\phi = \frac{\pi}{2}$ for ease of calculation, as we know from Section 3 that this choice recovers the correct MS unitary in the absence of the carrier transition. We also define $\Delta \equiv \delta + \nu_0$ for ease of notation. This yields:

$$\tilde{H}_{int} = \frac{i\hbar\Omega_R}{2}\hat{S}_+(e^{i\Delta t} + e^{-i\Delta t}) + h.c. + \text{sideband terms.} \tag{41}$$

For now we only care about the transition $|gg\rangle \leftrightarrow |ee\rangle$. We will work in the reduced basis of $\{|gg,n\rangle, |ge,n\rangle, |eg,n\rangle, |ee,n\rangle\}$ such that we only consider the carrier transition effects (the sideband terms for the core MS interaction will be added in later). The goal will be to obtain and solve differential equations for the probability amplitudes c_{ggn} and c_{een} defined by the Schrodinger equation:

$$i\frac{d}{dt}\vec{c} = \frac{1}{\hbar}\tilde{H}_{int}\vec{c} \tag{42}$$

The relevant matrix elements will therefore be given by:

$$\langle eg,n|\tilde{H}_{int}|gg,n\rangle, \langle ge,n|\tilde{H}_{int}|gg,n\rangle, \langle ee,n|\tilde{H}_{int}|ge,n\rangle, \langle ee,n|\tilde{H}_{int}|eg,n\rangle \tag{43}$$

By considering the form of the Hamiltonian, we see that these will all be equivalent, given by:

$$\frac{i\hbar\Omega_R}{2}(e^{i\Delta t} + e^{-i\Delta t}) = i\hbar\Omega_R\cos(\Delta t) \tag{44}$$

In order to solve for c_{ggn} and c_{een} in the presence of the carrier transition, we will first require the time evolution of amplitudes c_{gen} and c_{egn} in terms of c_{ggn} and c_{een}. Substituting in the matrix elements obtained in (44) to the corresponding Schrodinger equations for these states (where we assume that all states other than $|gg,n\rangle$ and $|ee,n\rangle$ are never meaningfully populated), we obtain:

$$\frac{d}{dt}c_{gen} = \frac{d}{dt}c_{egn} = \Omega_R\cos(\Delta t)(c_{ggn} - c_{een}) \tag{45}$$

Thus, $c_{gen}(t)$ and $c_{egn}(t)$ can be obtained by integrating (45):

$$c_{gen}(t) - c_{gen}(0) = c_{egn}(t) - c_{egn}(0) = \Omega_R\int_0^t dt'\cos(\Delta t')(c_{ggn}(t') - c_{een}(t')) \tag{46}$$

To obtain the particular mapping for input $|ee,n\rangle$, we take the states $|ge,n\rangle$ and $|eg,n\rangle$ to be initially unpopulated. Thus, we can set $c_{gen}(0) = c_{egn}(0) = 0$.

We now take the adiabatic limit, where Δ is assumed to be much larger than the effective Rabi frequency Ω for the MS gate oscillations. In this limit, we assume that $c_{ggn}(t)$ and $c_{een}(t)$ will remain roughly constant within one cycle of oscillations at the fast frequency Δ, as the timescale of the MS gate dynamics is much slower at frequency Ω. To first order, within the k^{th} cycle at frequency Δ:

$$c_{ggn}(t) \approx c_{ggn}(t_k) + (t - t_k)\dot{c}_{ggn}(t_k) \tag{47}$$

We divide the integral in (46) into a sum of smaller integrals over each full oscillation at the fast frequency Δ, then add the residual term leftover at the end after the final complete cycle. Defining T_k to be the time at the end of the last complete oscillation at frequency Δ, we obtain:

$$
\begin{aligned}
c_{gen}(t) = & \sum_{k=0}^{\#\text{full cycles}-1} \Omega_R \int_{t_k}^{t_k+\frac{2\pi}{\Delta}} dt' \cos(\Delta t')(c_{ggn}(t') - c_{een}(t')) \\
& + \Omega_R \int_{T_k}^{t} dt' \cos(\Delta t')(c_{ggn}(t') - c_{een}(t'))
\end{aligned}
\tag{48}
$$

First we consider the sum over complete cycles. Substituting in (47), we obtain:

$$
\begin{aligned}
c_{gen}(T_k) &= \Omega_R \sum_k \int_{t_k}^{t_k+\frac{2\pi}{\Delta}} \cos(\Delta t')(c_{ggn}(t_k) + (t-t_k)\dot{c}_{ggn}(t_k) - c_{een}(t_k) - (t-t_k)\dot{c}_{een}(t_k))dt' \\
&= \Omega_R \sum_k \int_0^{\frac{2\pi}{\Delta}} t' \cos(\Delta t')(\dot{c}_{ggn}(t_k) - \dot{c}_{een}(t_k))dt'
\end{aligned}
\tag{49}
$$

Integrating by parts, we find that this contribution at first order will vanish exactly. This is a consequence of the symmetry of the detuning from the two sidebands. The physical interpretation of this cancellation is that there will be no leading order AC Stark shift due to the carrier transition [6][7]. We therefore need to expand to second order:

$$
\begin{aligned}
c_{gen}(T_k) &= \Omega_R \sum_k \int_{t_k}^{t_k+\frac{2\pi}{\Delta}} \cos(\Delta t')(\frac{1}{2}(t-t_k)^2\ddot{c}_{ggn}(t_k) - \frac{1}{2}(t-t_k)^2\ddot{c}_{een}(t_k))dt' \\
&= \frac{\Omega_R}{2} \sum_k \int_0^{\frac{2\pi}{\Delta}} t'^2 \cos(\Delta t')(\ddot{c}_{ggn}(t_k) - \ddot{c}_{een}(t_k))dt' \\
&= \frac{\Omega_R}{2} \sum_k \frac{4\pi}{\Delta^3}(\ddot{c}_{ggn}(t_k) - \ddot{c}_{een}(t_k))
\end{aligned}
\tag{50}
$$

In the limit of small $\frac{4\pi}{\Delta}$ relative to the timescale of variation in $c_{ggn}(t)$ and $c_{een}(t)$, this sum tends to an integral:

$$
\begin{aligned}
c_{gen}(T_k) &= \frac{\Omega_R}{2} \sum_k \frac{4\pi}{\Delta^3}(\ddot{c}_{ggn}(t_k) - \ddot{c}_{een}(t_k)) \\
&\to \frac{\Omega_R}{2} \cdot \frac{2}{\Delta^2} \int_0^{T_k} dt'(\ddot{c}_{ggn}(t') - \ddot{c}_{een}(t')) \\
&= \frac{\Omega_R}{\Delta^2}(\dot{c}_{ggn}(T_k) - \dot{c}_{een}(T_k))
\end{aligned}
\tag{51}
$$

We now account for the residual part after all complete cycles. For consistency with above, we again expand to second order:

$$
\begin{aligned}
c_{gen}(t) - c_{gen}(T_k) &= \Omega_R \int_{T_k}^{t} dt' \cos(\Delta t')(c_{ggn}(t') - c_{een}(t')) \\
&= \Omega_R \int_0^{t'-T_k} \cos(\Delta t')(c_{ggn}(T_k) - c_{een}(T_k))dt' \\
&\quad + \Omega_R \int_0^{t-T_k} t' \cos(\Delta t')(\dot{c}_{ggn}(T_k) - \dot{c}_{een}(T_k))dt' \\
&\quad + \frac{\Omega_R}{2} \int_0^{t-T_k} t'^2 \cos(\Delta t')(\ddot{c}_{ggn}(T_k) - \ddot{c}_{een}(T_k))dt' \\
&= \Omega_R(c_{ggn}(T_k) - c_{een}(T_k))\frac{\sin(\Delta t)}{\Delta} \\
&\quad + \Omega_R(\dot{c}_{ggn}(T_k) - \dot{c}_{een}(T_k))(\frac{t-T_k}{\Delta}\sin(\Delta t) + \frac{1}{\Delta^2}\cos(\Delta t) - \frac{1}{\Delta^2}) \\
&\quad + \frac{\Omega_R}{2}(\ddot{c}_{ggn}(T_k) - \ddot{c}_{een}(T_k))(\frac{(t-T_k)^2}{\Delta}\sin(\Delta t) + \frac{2(t-T_k)}{\Delta^2}\cos(\Delta t) - \frac{2}{\Delta^3}\sin(\Delta t))
\end{aligned} \tag{52}
$$

Adding this to the result of (51), we obtain:

$$
\begin{aligned}
c_{gen}(t) &= \Omega_R(c_{ggn}(T_k) - c_{een}(T_k))\frac{\sin(\Delta t)}{\Delta} \\
&\quad + \Omega_R(\dot{c}_{ggn}(T_k) - \dot{c}_{een}(T_k))(\frac{t-T_k}{\Delta}\sin(\Delta t) + \frac{1}{\Delta^2}\cos(\Delta t) - \frac{1}{\Delta^2} + \frac{1}{\Delta^2}) \\
&\quad + \frac{\Omega_R}{2}(\ddot{c}_{ggn}(T_k) - \ddot{c}_{een}(T_k))(\frac{(t-T_k)^2}{\Delta}\sin(\Delta t) + \frac{2(t-T_k)}{\Delta^2}\cos(\Delta t) - \frac{2}{\Delta^3}\sin(\Delta t)) \\
&= \frac{\Omega_R}{\Delta}\sin(\Delta t)(c_{ggn}(T_k) + (t-T_k)\dot{c}_{ggn}(T_k) + \frac{1}{2}(t-T_k)^2\ddot{c}_{ggn}(T_k) + \ldots) \\
&\quad - \frac{\Omega_R}{\Delta}\sin(\Delta t)(c_{een}(T_k) + (t-T_k)\dot{c}_{een}(T_k) + \frac{1}{2}(t-T_k)^2\ddot{c}_{een}(T_k) + \ldots) \\
&\quad + \frac{\Omega_R}{\Delta^2}\cos(\Delta t)((\dot{c}_{ggn}(T_k) - \dot{c}_{een}(T_k)) + (t-T_k)(\ddot{c}_{ggn}(T_k) - \ddot{c}_{een}(T_k)) + \ldots) \\
&\quad + O(\frac{\Omega_R}{\Delta^3}) \\
&= \frac{\Omega_R}{\Delta}\sin(\Delta t)(c_{ggn}(t) - c_{een}(t)) + \frac{\Omega_R}{\Delta^2}\cos(\Delta t)(\dot{c}_{ggn}(t) - \dot{c}_{een}(t)) + \ldots
\end{aligned} \tag{53}
$$

Thus, we obtain a leading order expression for $c_{gen}(t)$ (and the equivalent result for $c_{egn}(t)$) in terms of $c_{ggn}(t)$ and $c_{een}(t)$. Substituting these into the Schrodinger equations for $c_{ggn}(t)$ and $c_{een}(t)$ allows us to obtain a set of coupled linear differential equations for this subspace. For a more rigorous analysis, we will also require the full matrix element contributions from the sideband terms containing $c_{ge,n\pm1}$ and $c_{eg,n\pm1}$, however, for simplicity, we assume that the MS interaction generated by the sideband transitions can be well-approximated by simple Rabi oscillations at the previously defined effective Rabi frequency Ω. Thus, for the purposes of finding the leading order effects of the carrier transition, we neglect the motion of the phonon states in phase space, and the additional $-\sin(\delta t)$ term in the propagator for the entangling MS interaction. This result will be equivalent to adiabatically eliminating the amplitudes $c_{ge,n\pm1}$ and $c_{eg,n\pm1}$ by taking them to be sufficiently off-resonant that they are never meaningfully populated. Thus, ignoring the carrier terms for now, the dynamics we obtain from the MS interaction will approximately be given by:

$$\begin{cases} i\dot{c}_{een} = \Omega(c_{ggn} + c_{een}) \\ i\dot{c}_{ggn} = \Omega(c_{ggn} + c_{een}) \end{cases} \tag{54}$$

Now accounting for the carrier terms:

$$\begin{cases} i\dot{c}_{een} = \Omega(c_{ggn} + c_{een}) + i\hbar\Omega_R \cos(\Delta t)(c_{egn} + c_{gen}) \\ i\dot{c}_{ggn} = \Omega(c_{ggn} + c_{een}) - i\hbar\Omega_R \cos(\Delta t)(c_{egn} + c_{gen}) \end{cases} \tag{55}$$

Substituting in the results of (53), we obtain:

$$\begin{cases} i\dot{c}_{een} = \Omega(c_{ggn} + c_{een}) + \frac{i{\Omega_R}^2}{\Delta}\sin(2\Delta t)(c_{ggn} - c_{een}) + \frac{2i{\Omega_R}^2}{\Delta^2}\cos^2(\Delta t)(\dot{c}_{ggn} - \dot{c}_{een}) \\ i\dot{c}_{ggn} = \Omega(c_{ggn} + c_{een}) - \frac{i{\Omega_R}^2}{\Delta}\sin(2\Delta t)(c_{ggn} - c_{een}) - \frac{2i{\Omega_R}^2}{\Delta^2}\cos^2(\Delta t)(\dot{c}_{ggn} - \dot{c}_{een}) \end{cases} \tag{56}$$

For ease of notation, we define $f(t) \equiv \frac{2{\Omega_R}^2}{\Delta^2}\cos^2(\Delta t)$ and $g(t) \equiv i\frac{{\Omega_R}^2}{\Delta}\sin(2\Delta t)$. Expressing (56) in matrix form:

$$\begin{aligned} i\dot{\vec{c}} &= \Omega \begin{pmatrix} 1 & 1 \\ 1 & 1 \end{pmatrix} + g(t) \begin{pmatrix} 1 & -1 \\ -1 & 1 \end{pmatrix} \vec{c} + if(t) \begin{pmatrix} 1 & -1 \\ -1 & 1 \end{pmatrix} \dot{\vec{c}} \\ \implies i &\begin{pmatrix} 1 - f(t) & f(t) \\ f(t) & 1 - f(t) \end{pmatrix} \dot{\vec{c}} = \begin{pmatrix} \Omega + g(t) & \Omega - g(t) \\ \Omega - g(t) & \Omega + g(t) \end{pmatrix} \vec{c} \end{aligned} \tag{57}$$

By observation, the basis $\{|\pm\rangle\}$ (defined here by $|\pm\rangle \equiv \frac{|ee\rangle \pm |gg\rangle}{\sqrt{2}}$) will diagonalise this system. Re-expressing the matrices in this basis, we obtain:

$$i \begin{pmatrix} 1 & 0 \\ 0 & 1 - 2f(t) \end{pmatrix} \dot{\vec{c}} = \begin{pmatrix} 2\Omega & 0 \\ 0 & 2g(t) \end{pmatrix} \vec{c} \tag{58}$$

Solving this decoupled system yields:

$$c_+(t) = c_+(0)\exp(-2i\Omega t) \tag{59}$$

$$c_-(t) = c_-(0)\sqrt{\frac{1 - 4\alpha\cos^2(\Delta t)}{1 - 4\alpha}}, \tag{60}$$

where $\alpha = \frac{{\Omega_R}^2}{\Delta^2}$. Expanding for small α:

$$\begin{aligned} c_-(t) &= c_-(0)(1 - 2\alpha\cos^2(\Delta t))(1 + 2\alpha) \\ &= c_-(0)(1 + 2\alpha\sin^2(\Delta t)) + O(\alpha^2) \end{aligned} \tag{61}$$

Thus, taking the particular input of $c_{een}(0) = 1$, we can take the initial conditions $c_+ = c_- = \frac{1}{\sqrt{2}}$. Lastly, we can now combine the results of $c_+(t)$ and $c_-(t)$ to obtain the dynamics of $c_{een}(t)$:

$$\begin{aligned} c_{een}(t) &= \frac{1}{\sqrt{2}}(c_+(t) + c_-(t)) \\ &= \frac{1}{2}(e^{-2i\Omega t} + 1 + 2\alpha \sin^2(\Delta t)) \\ &= \frac{e^{-i\Omega t}}{2}(e^{-i\Omega t} + e^{i\Omega t} + 2\alpha e^{i\Omega t}\sin^2(\Delta t)) \\ &= e^{-i\Omega t}(\cos(\Omega t) + \alpha e^{i\Omega t}\sin^2(\Delta t)) \end{aligned} \tag{62}$$

And similarly, for $c_{ggn}(t)$:

$$\begin{aligned} c_{ggn}(t) &= \frac{1}{\sqrt{2}}(c_+(t) - c_-(t)) \\ &= e^{-i\Omega t}(-i\sin(\Omega t) - \alpha e^{i\Omega t}\sin^2(\Delta t)) \end{aligned} \tag{63}$$

Thus, ignoring the global phase, we again obtain Rabi oscillations at frequency Ω giving the familiar MS gate mappings at $\Omega t = \frac{\pi}{4}$. However, this becomes superposed by fast oscillations at frequency Δ and with amplitude $\alpha = \frac{{\Omega_R}^2}{\Delta^2}$. This justifies the prior claim that as we increase the Rabi frequency relative to the carrier detuning, the effects of the carrier transition become more dominant in the dynamics of the system, and in particular we find that these effects will scale quadratically with this ratio.

5.2 Verification of Carrier Transition Effects

To test the validity of the result obtained in (63), we consider how the fidelity of the gate changes as Ω_R is varied such that Δt is chosen to be an integer or half-integer multiple of π. We expect that for integer multiples of π, the carrier effects should be eliminated up to order α, whereas for the half-integer case, we should expect the gate infidelity to increase quadratically with $\frac{\Omega_R}{\Delta}$ (assuming loop closure and other conditions listed at the start of Section 4 are met). Although experimentally, this level of precision is typically not attainable, arbitrary precision is possible within a numerical simulation, thus we test this prediction using a Lindblad master equation solver run on the Hamiltonian given in (40). Figure 6 shows the results obtained for the integer and half-integer cases. Figure 7 shows visible fast oscillations in the expectation value of $\hat{\sigma}_z$ in the $\{|gg\rangle, |ee\rangle\}$ subspace.

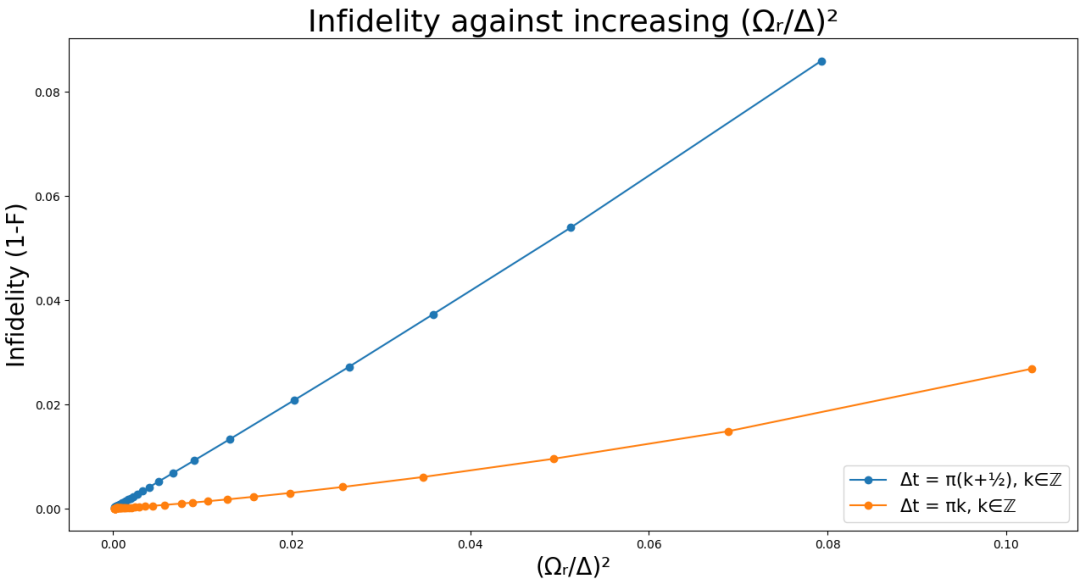

Figure 6: The infidelities for the mappings of $|gg\rangle$ to $\frac{1}{\sqrt{2}}(|gg\rangle - i|ee\rangle)$ are seen to increase linearly with $(\frac{\Omega_R}{\Delta})^2$ when $\Delta t_g = (k + \frac{1}{2})\pi, k \in \mathbb{Z}$. This is consistent with what we expect from (62,63). However, contrary to the predictions of (62,63), we also see a smaller but non-negligible rise in the infidelity for integer multiples of π. This can partly be explained by excitations of the off-resonant sidebands, where the red detuned laser excites the blue sideband and vice versa to a non-negligible degree. These will be the next most dominant effects to consider, being smaller only by a factor of η. Further, for larger Ω_R, we also expect terms of order $(\frac{\Omega_R}{\Delta})^4$ to begin to contribute to the dynamics, which already become non-negligible at ~ 0.01 for $\frac{\Omega_R}{\Delta} \sim 0.1$.

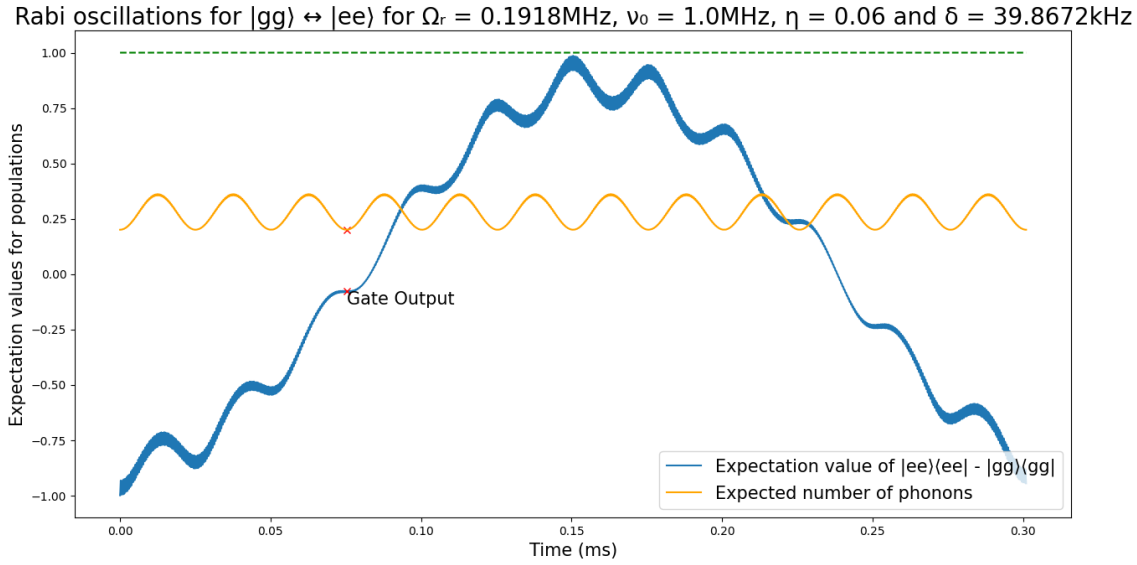

Figure 7: Off-resonant Rabi oscillations at frequency Δ visible for larger Ω_R. We observe that the amplitude of these oscillations appears modulated with the slow oscillations at frequency Ω, such that they are largest for $\Omega t = 0, \frac{\pi}{2}, \pi$, and are smaller at the gate output time. This is due to the variation of the phase of these oscillations with Ωt, as predicted by (62,63). Note this plot also shows fast oscillations due to the far off-resonant sideband transitions which are superposed onto the carrier oscillations, which explains why the visible oscillations are reduced, but do not completely vanish at the gate time.

6 Other noise sources

Thus far, we have focused largely on error sources that are inherent to the original Hamiltonian stated in (10). These have arisen by virtue of the fundamental dynamics of the laser-ion interaction not being exactly the MS interaction we want to construct. These errors include (but are not limited to) [3]:

- Higher order terms in the Lamb-Dicke expansion of $O(\eta^2)$.
- Off-resonant phonon modes beyond just the centre-of-mass mode considered here. In the literature, these are often referred to as 'spectator modes' [3].
- Off-resonant excitations of transitions such as the carrier and far off-resonant sidebands. These may induce unwanted fast oscillations (as seen in Section 5) and AC Stark shifts.
- Errors resulting from imperfect tuning of pulse lengths, detunings, laser amplitudes and phase.

In this section, we will focus instead on external error sources that have not already been accounted for in the Hamiltonian. The effects we will analyse here are given by the following (note this is again not an exhaustive list, but it is sufficiently broad for giving insight into the key noise mechanisms for trapped-ion qubits):

- Spontaneous emission between the electronic logical qubit levels. In the case of hyperfine or Zeeman qubits, where the logical states are connected via Raman transitions, spontaneous emission from this Raman virtual level will need to be considered instead.
- Dephasing due to stray electric and magnetic field noise.
- Heating of the motional phonon modes due to electric field noise.

For each of the above processes, we will derive physically their impacts on the system using the formalism of quantum noise and quantum operations. A more in depth discussion of the theory of quantum operations in open systems is provided in [1], but a short summary of the key results will be derived in the following. We will then use this formalism to describe and analyse the dynamics resulting from each of the above effects.

6.1 Operator-sum representation of open systems

We provide here a short overview of what is known as the *operator-sum representation* [1] for describing the dynamics of open quantum systems. This is a useful formalism for analysing the dynamics of a system weakly coupled to its environment, without needing to model the entire joint system including the environment Hilbert space. Thus it becomes a very useful tool for describing and understanding the effects of noise in quantum channels.

Consider some system S with state given by the density matrix ρ_S. We are interested in finding the dynamics of ρ_S, which in the absence of any noise, we know will be governed by the von Neumann equation $\frac{d}{dt}\rho = -\frac{i}{\hbar}[H, \rho]$, where H is the Hamiltonian for the space S. However, suppose now that the space S is weakly coupled to its environment, described also by some Hilbert space which we will denote E. We now will instead be dealing with the joint system $S \otimes E$, which in general will undergo some unitary evolution $U_{tot}(t)$ due to the overall Hamiltonian of the joint system. We still want to find the dynamics of ρ_S, which we obtain by taking a partial trace over the environment space:

$$\rho_S(t) = tr_{env}(U_{tot}\rho_{(S\otimes E)}U_{tot}^\dagger) \tag{64}$$

The presence of interactions with the environment has important consequences for the dynamics of ρ_S, most notably that it need not necessarily be strictly unitary anymore. We will show here that the resulting dynamics can be represented in what is called the *operator-sum* or *Kraus* representation for quantum operations. To obtain this, we first make two simplifying assumptions about the joint system. Firstly, the intial state of $\rho_{(S\otimes E)}$ is assumed to be a product state $\rho_S(0) \otimes \rho_E(0)$. This assumption will be valid for quantum computing setups where initial states of the system are prepared and correlations with the environment are destroyed at $t = 0$. Secondly, the environment state is assumed to be initially some pure state $|e_0\rangle$, rather than a general mixed state. This requirement can always be satisfied by expanding the environment space E and 'purifying' the density matrix into a pure state. Taking these two assumptions to be met, we define the basis $\{|e_k\rangle\}$ to span the environment space E in order to take the partial trace, and can obtain the dynamics for ρ_S in the following [1][12]:

$$\begin{aligned}\rho_S(t) &= tr_{env}(U_{tot}(\rho_S \otimes |e_0\rangle\langle e_0|)U_{tot}^\dagger) \\ &= \sum_k \langle e_k|U_{tot}(\rho_S \otimes |e_0\rangle\langle e_0|)U_{tot}^\dagger|e_k\rangle \\ &= \sum_k E_k \rho_S E_k^\dagger,\end{aligned} \tag{65}$$

where $E_k \equiv \langle e_k|U_{tot}|e_0\rangle$ are operators that by construction will only act on the system space S. These operators are called *operation elements* or *Kraus operators*, and the summation of the result of acting on ρ_S with these operators gives the *operator-sum representation* for describing the resulting quantum operation on ρ_S. We now proceed by applying this formalism to the specific noise processes listed above, by finding specific instances of these operation elements in each case.

6.2 Spontaneous Emission

We want to obtain operation elements E_k for spontaneous emission in order to obtain its operator-sum representation. To do this, we will need to consider the open system dynamics of each ion with the radiation field [9]. Up until this point we have adopted an entirely semi-classical picture, where the interaction Hamiltonian is assumed to take the form of an electric dipole perturbation $-\hat{d} \cdot \vec{E}$ for some electric dipole operator $\hat{d} \equiv -e\hat{r}$ and a classically well-defined electric field $\vec{E}$. This picture works well, as quantum properties of the radiation field become extremely well-approximated by the classical electromagnetic wave treatment for the strong coherent lasers that we deal with here. However, the semi-classical picture misses the phenomenon of *spontaneous emission*, which can only be described properly when we consider the coupling of the ion to the quantised radiation field [9]. The result of this is that we obtain non-zero matrix elements in the interaction Hamiltonian between multipole-connected electronic levels of the ion even in the absence of any photons, such that by Fermi's golden rule, the ion may *spontaneously* emit a photon and decay into the lower energy state without being driven by a laser. A full QED treatment to recover this process is obviously overkill and wholly impractical, which motivates applying the quantum operation formalism as derived above for this process.

Let $|g, 0\rangle$ denote a state in the ground electronic state and with 0 photons (not phonons, these are not considered for the moment) in a particular mode with energy $\hbar\omega_0$ in the environment space. Even when allowing for spontaneous emission, this state will remain in this state indefinitely, as in the two-level picture we assume there are no lower-energy multipole-connected states that it can decay to. However, in some time t, the excited state $|e, 0\rangle$ may spontaneously decay via emission of a photon to

the state $|g,1\rangle$ with some probability p, or remain in the state $|e,0\rangle$ with probability $(1-p)$. Tracing over the environment, we therefore obtain for final photon states $|0\rangle$ and $|1\rangle$ respectively:

$$E_0 = \begin{pmatrix} 1 & 0 \\ 0 & \sqrt{1-p} \end{pmatrix}, \quad E_1 = \begin{pmatrix} 0 & \sqrt{p} \\ 0 & 0 \end{pmatrix} \tag{66}$$

The resulting quantum operation is known as *amplitude damping*. The operation element E_0 can be interpreted as leaving the state $|g\rangle$ unchanged, whilst reducing the amplitude of $|e\rangle$ by a factor of $\sqrt{1-p}$. The operation element E_1 can be interpreted as decaying the state $|e\rangle$ to $|g\rangle$, losing energy to the environment. Operating on ρ with these operation elements yields:

$$\begin{aligned} &\begin{pmatrix} 1 & 0 \\ 0 & \sqrt{1-p} \end{pmatrix} \begin{pmatrix} \rho_{00} & \rho_{01} \\ \rho_{10} & \rho_{11} \end{pmatrix} \begin{pmatrix} 1 & 0 \\ 0 & \sqrt{1-p} \end{pmatrix} + \begin{pmatrix} 0 & \sqrt{p} \\ 0 & 0 \end{pmatrix} \begin{pmatrix} \rho_{00} & \rho_{01} \\ \rho_{10} & \rho_{11} \end{pmatrix} \begin{pmatrix} 0 & 0 \\ \sqrt{p} & 0 \end{pmatrix} \\ &= \begin{pmatrix} \rho_{00} & \rho_{01}\sqrt{1-p} \\ \rho_{10}\sqrt{1-p} & \rho_{11}(1-p) \end{pmatrix} + \begin{pmatrix} \rho_{11}p & 0 \\ 0 & 0 \end{pmatrix} \\ &= \begin{pmatrix} \rho_{00}+\rho_{11}p & \rho_{01}\sqrt{1-p} \\ \rho_{10}\sqrt{1-p} & \rho_{11}(1-p) \end{pmatrix} \end{aligned} \tag{67}$$

Thus we obtain that the effect of spontaneous emission will be to map states towards the ground state $|g\rangle$ and to exponentially decay coherences between the $|g\rangle$ and $|e\rangle$ states. Note the trace of the density matrix is necessarily preserved in this operation, ensuring that we still obtain a valid normalised density matrix after spontaneous emission.

We now reintroduce the bichromatic driving lasers to the system's dynamics in order to understand spontaneous emission within the context of the MS gate operation. Figure 8 demonstrates the results obtained for various decay rates in the regime where the frequency of the gate Rabi oscillations Ω is taken to be much faster than the rate of spontaneous emission γ (such that the ions do not all converge to the ground state). This regime is consistent with observed rates of spontaneous emission for real trapped-ion setups; for example, the decay time (defined by the time taken for the population of $|e\rangle$ to decay to $\frac{1}{e}$ of its initial value) for the excited level in the optical qubit used in the $^{40}Ca^{+}$ setup we considered in Section 4 was found to be 1.1 seconds, which is many orders of magnitude greater than typical gate times, which are of the order of microseconds [3][11]. For Zeeman and hyperfine qubits, the decay times are even longer, and are typically many orders of magnitude greater than any experimentally relevant timescales, such that its impact as a noise process becomes completely negligible [3]. Thus, we conclude that spontaneous emission is consequently far less significant than the other noise sources we will later consider, and is therefore typically not the most dominant experimental bottleneck for the construction of high fidelity gates.

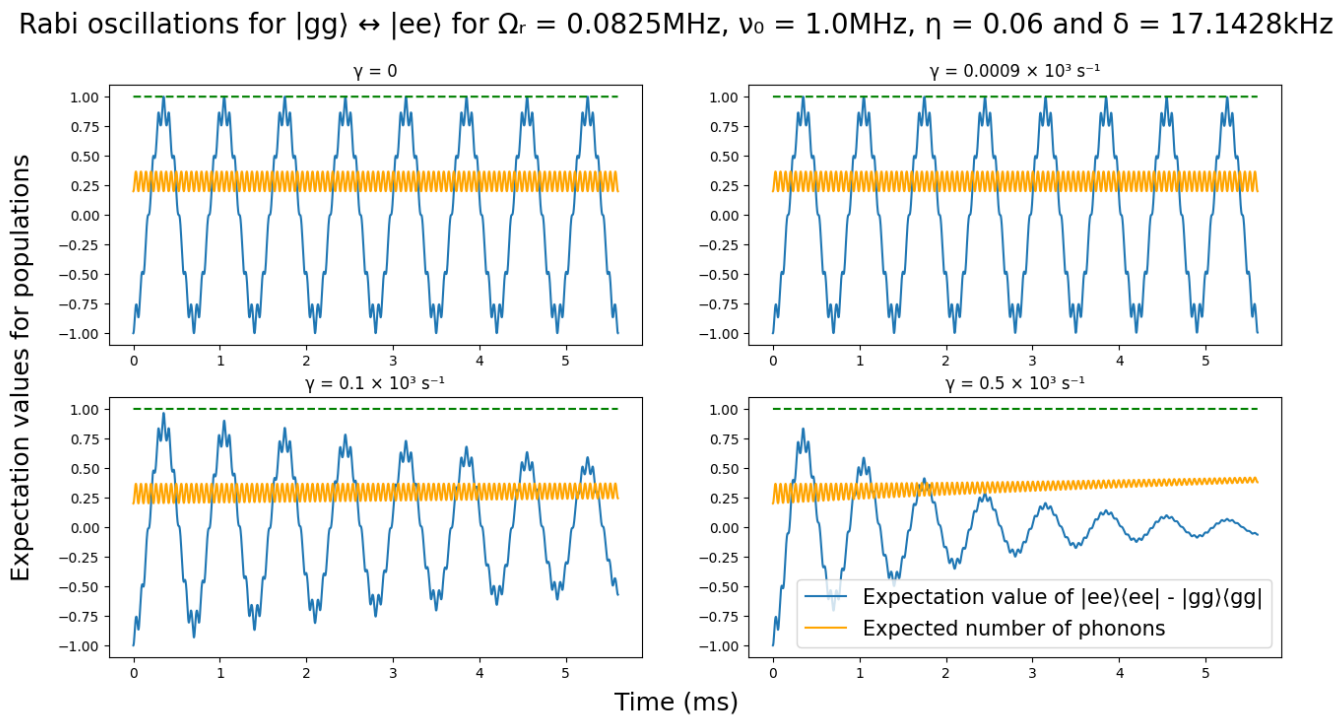

Figure 8: MS gate Rabi oscillations obtained for initial state $|gg\rangle$ in the presence of spontaneous emission for different decay rates γ. The top right graph shows the results obtained for the decay rate in the $^{40}Ca^{+}$ optical qubit. We observe that spontaneous emission has the effect of exponentially reducing the amplitude of oscillations over time. The plots are obtained using a Lindblad master equation solver in QuTip (the simulation used can be found on my GitHub page), where the Hamiltonian is taken to be the simplified form obtained in (19) after the second RWA is applied to kill the carrier and far off-resonant sidebands. The Lindblad collapse operator for spontaneous emission is given by $\hat{L}_{se} = \sqrt{\gamma}|g\rangle\langle e|$.

6.3 Dephasing

We consider here the effects of magnetic field and slow electric field noise on the system dynamics. We will consider each of these effects in turn, and will find that both will lead to *dephasing*, or *phase damping*, which we will derive in the following. First we consider the impacts of stray magnetic fields interacting with the ions. These will induce a magnetic dipole term in the Hamiltonian given by $-\vec{\mu}\cdot\vec{B}$, where $\vec{\mu}$ gives the magnetic moment of the ion for a given electronic state. Dephasing occurs when the strength of this $\vec{B}$ field is not accounted for, and leads to the accumulation of relative phase between states with different $\vec{\mu}$ [3].

To illustrate the effects of phase damping, we take the qubit space spanned by $|g\rangle$ and $|e\rangle$, and assume for the moment that we have no external perturbation aside from the dephasing noise process we will consider, such that in the interaction picture both states will remain static with no phase accrual over time. Introducing now the magnetic dipole interaction, we assume the effect of this will be some non-zero additional energy splitting between these states such that in some time Δt, $|e\rangle$ will gain additional phase $e^{i\theta_B}$ relative to $|g\rangle$. As a simplifying assumption, we take the $\vec{B}$ field to vary in such a way that θ_B will become well-represented by some continuous random variable [1], and further, central limit theorem tells us that this will tend to a normal distribution for large times Δt. Thus, taking the mean to be 0 and the variance 2λ for this distribution, we can obtain the expectation for the resulting density matrix after time Δt:

$$
\begin{aligned}
\rho(\Delta t) &= \frac{1}{\sqrt{4\pi\lambda}} \int_{-\infty}^{\infty} d\theta_B R_z(\theta_B)\rho(0)R_z^{\dagger}(\theta_B)\exp(-\frac{\theta_B^2}{4\lambda}) \\
&= \frac{1}{\sqrt{4\pi\lambda}} \int_{-\infty}^{\infty} d\theta_B \begin{pmatrix} 1 & 0 \\ 0 & e^{i\theta_B} \end{pmatrix} \begin{pmatrix} \rho_{00} & \rho_{01} \\ \rho_{10} & \rho_{11} \end{pmatrix} \begin{pmatrix} 1 & 0 \\ 0 & e^{-i\theta_B} \end{pmatrix} \exp(-\frac{\theta_B^2}{4\lambda}) \\
&= \frac{1}{\sqrt{4\pi\lambda}} \int_{-\infty}^{\infty} d\theta_B \begin{pmatrix} \rho_{00} & \rho_{01}e^{-i\theta_B} \\ \rho_{10}e^{i\theta_B} & \rho_{11} \end{pmatrix} \exp(-\frac{\theta_B^2}{4\lambda}) \\
&= \begin{pmatrix} \rho_{00} & \rho_{01}e^{-\lambda} \\ \rho_{10}e^{-\lambda} & \rho_{11} \end{pmatrix}
\end{aligned}
\tag{68}
$$

We infer from (68) that the result of dephasing will be exponential decay of off-diagonal elements of the density matrix, such that for large times Δt (and therefore large variance 2λ), any superposition state $\alpha|g\rangle + \beta|e\rangle$ will tend to the mixed state $|\alpha|^2|g\rangle\langle g| + |\beta|^2|e\rangle\langle e|$. This will result in the loss of any coherence properties of the superposition.

Applying this noise process to the MS gate dynamics, we obtain similar results to the plots obtained from spontaneous emission. The results can be seen in Figure 9. As with spontaneous emission, we see that phase damping has the effect of exponentially reducing the amplitude of oscillations over time, however, phase damping will differ from spontaneous emission in that rather than pulling each ion towards the ground state $|g\rangle$, the steady state solution for the density matrix of each ion will be the maximal entropy state $\frac{1}{2}(|g\rangle\langle g| + |e\rangle\langle e|)$. This solution arises physically due to the gradual loss of coherence between the $|g\rangle$ and $|e\rangle$ states, whilst Rabi oscillations of each ensure that we become equally probable to observe any state for either ion at large times. We also interestingly observe the gradual increase of the number of phonons over time. This arises by consequence of the decoherence between the $|g\rangle$ and $|e\rangle$ states causing the loop closure condition for the displacement operator to no longer be valid, such that the initial motional state is no longer cleanly recovered after every cycle.

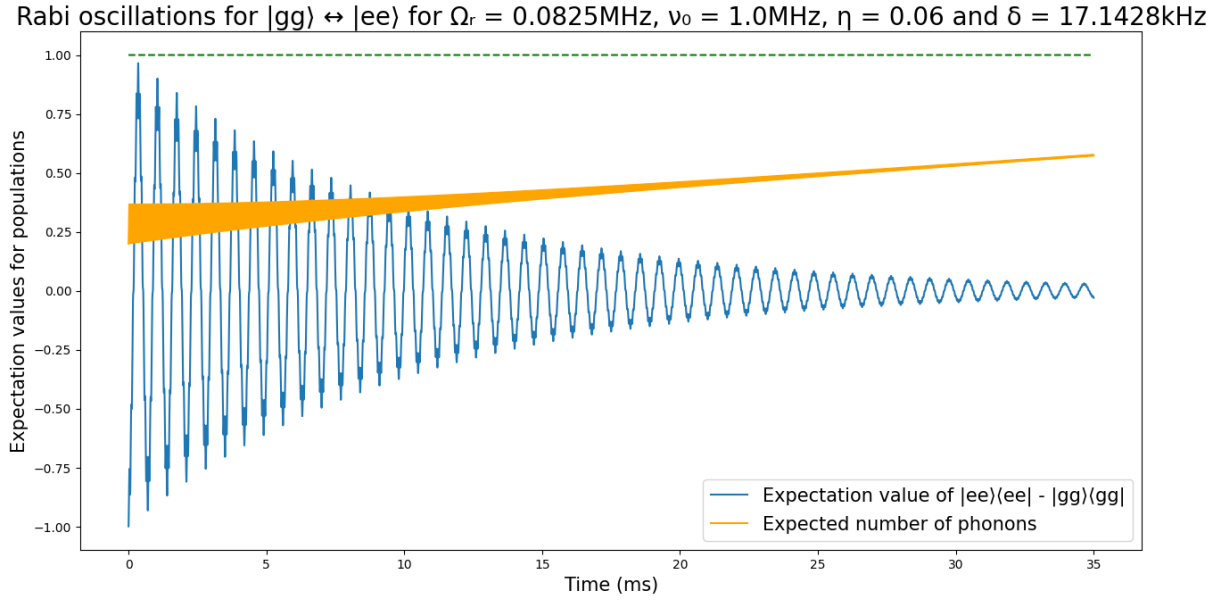

Figure 9: MS gate Rabi oscillations obtained for initial state $|gg\rangle$ in the presence of phase damping. The corresponding Lindblad operator is given by $\hat{L}_{pd} = \sqrt{\gamma}\hat{\sigma}_z$, where γ gives the rate of phase damping. This plot is obtained for a choice of $\gamma = 50\text{s}^{-1}$.

We have shown that stray fluctuating magnetic fields can lead to dephasing between the electronic qubit levels due to the magnetic dipole interaction. We now consider the effects of slow electric field noise, which will require reintroducing the previously neglected motional states of the ions to our model. The word slow in this context describes the frequency of the fluctuations relative to the trap frequencies $\sim \nu_0$. Fast electric field noise will be considered in the next subsection on motional heating, as we will find this has a physically different effect on the system.

Just as variations in the magnetic field resulted in small shifts of the energy splitting between the electronic qubit states $|g\rangle$ and $|e\rangle$, we find that small voltage fluctuations in the trap electrodes will lead to gradual changes in the allowed normal mode frequencies for the motion of ions within the trap [3][4]. Thus, the phonon energy spacing $\hbar\nu_0$ in the centre-of-mass mode used for the sideband transitions, as well as the energy spacings for other spectator modes will change. However, there is a critical distinction here from the magnetic dipole interaction case in that these variations will change not only the energies of the unperturbed Hamiltonian H_0, but also the eigenbasis itself. Fortunately, in the limit of slow fluctuations, the adiabatic theorem tells us that states will track the instantaneous eigenbasis of H_0 as it changes, such that a given phonon state will remain in the corresponding phonon state of the changing motional Hamiltonian. The result will be only a variation in the corresponding energies, which as seen before will lead to dephasing.

As with spontaneous emission, it will become useful to obtain an operator-sum representation for this process. Note there is no unique set of operation elements to describe a given operation, and often different choices of operation elements can lend different insight into its structure. One choice [12] for representing the phase damping operation is the set given by:

$$E_0 = \begin{pmatrix} \sqrt{1-\gamma} & 0 \\ 0 & \sqrt{1-\gamma} \end{pmatrix}, \quad E_1 = \begin{pmatrix} \sqrt{\gamma} & 0 \\ 0 & 0 \end{pmatrix}, \quad E_2 = \begin{pmatrix} 0 & 0 \\ 0 & \sqrt{\gamma} \end{pmatrix}, \tag{69}$$

which by explicitly operating on ρ we see will recover the same results as (68):

$$\begin{aligned} \sum_j E_j \rho E_j^\dagger &= E_0 \rho E_0^\dagger + E_1 \rho E_1^\dagger + E_2 \rho E_2^\dagger \\ &= (1-\gamma) \begin{pmatrix} \rho_{00} & \rho_{01} \\ \rho_{10} & \rho_{11} \end{pmatrix} + \begin{pmatrix} \gamma\rho_{00} & 0 \\ 0 & 0 \end{pmatrix} + \begin{pmatrix} 0 & 0 \\ 0 & \gamma\rho_{11} \end{pmatrix} \\ &= \begin{pmatrix} \rho_{00} & \rho_{01}(1-\gamma) \\ \rho_{10}(1-\gamma) & \rho_{11} \end{pmatrix} \end{aligned} \tag{70}$$

Equating $(1-\gamma)$ from (70) and $e^{-\lambda}$ from (68) yields the correct mappings for the phase damping operation under this set of operation elements. This choice of representation can be interpreted physically as arising from elastic scattering of a photon, such that the ion has some probability γ in some arbitrary time interval of interacting elastically with its environment, which we will take to be some thermal bath of photons. Defining the initial state of the environment state to be given by $|0_E\rangle$, we consider the mappings $|g, 0_E\rangle \to \sqrt{1-\gamma}|g, 0_E\rangle + \sqrt{\gamma}|g, 1_E\rangle$ and $|e, 0_E\rangle \to \sqrt{1-\gamma}|e, 0_E\rangle + \sqrt{\gamma}|e, 2_E\rangle$, where $|1_E\rangle$ and $|2_E\rangle$ give the 2 possible states of the scattered photons in the environment after interacting with the ion in state $|g\rangle$ and $|e\rangle$ respectively. In this picture, when tracing over the environment space, E_0 will be the operation element obtained when the photon was unscattered whilst E_1 and E_2 will give the operation elements corresponding to the events where the photon was scattered. In the literature, often this alternative picture is used instead to represent the dephasing process, thus it is insightful to see explicitly how both pictures will lead to equivalent dynamics for the system.

6.4 Motional Heating

For faster electric field fluctuations, the adiabatic theorem cannot be applied. When the frequency of these fluctuations becomes comparable to the trap frequencies $\sim \nu_0$, the result will be resonant driving of transitions between the different phonon states, such that the phonon population in different modes may be changed. This will cause heating of the motional state.

Sources of such heating include blackbody radiation (albeit to a very limited extent) and fundamental Johnson noise arising from the random motion of electrons in the electrodes at finite temperature [4][5]. However, the observed heating rates are typically much greater than the theoretical predictions arising from these two conventional sources, thus we conclude that there must exist other sources of heating unaccounted for. In the literature, this heating is referred to as *anomalous motional heating*, or AMH. Although the exact origin of AMH is still an active area of research, current models predict that AMH arises from surface effects [4] (rather than bulk properties) of the electrodes, and is largest for low frequencies, short surface-ion distances and high temperatures [5].

Figure 10 shows the Rabi oscillation plots in the presence of motional heating. Remarkably, the fidelity suffers minimally from this noise process by consequence of the relative insensitivity of the MS gate to the motional state of the ions [2]. It is notable that here we observe not only a robustness against the initial state of the phonon subspace, as we had previously argued from the loop closure condition, but also to some extent against changes to this subspace during the gate's execution.

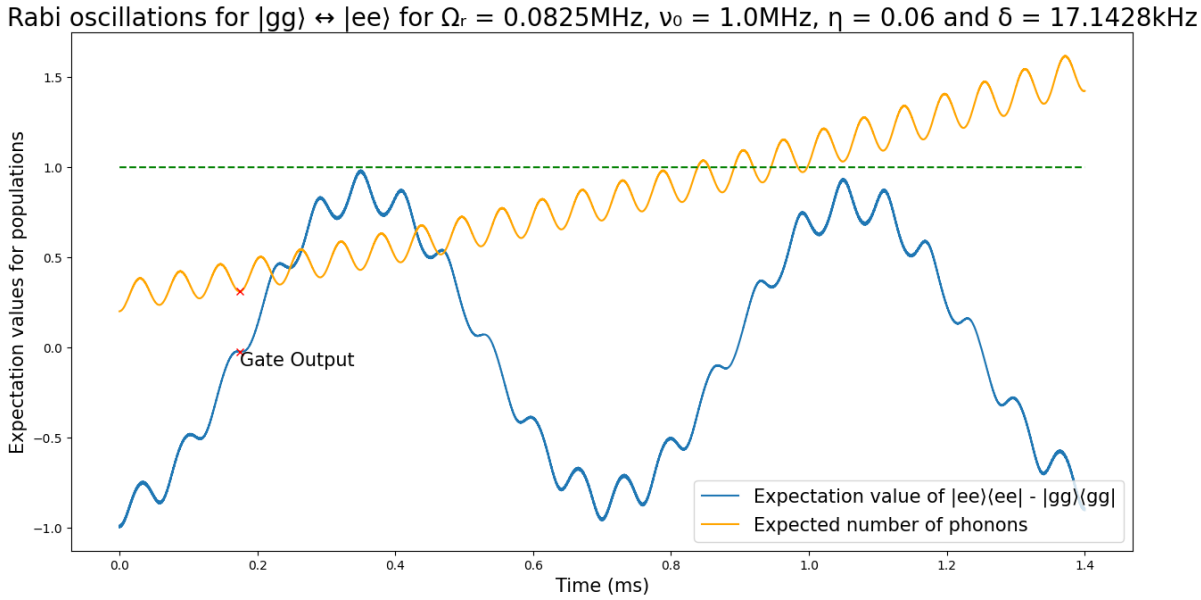

Figure 10: MS gate Rabi oscillations obtained for initial state $|gg\rangle$ in the presence of motional heating. The corresponding Lindblad operator is given by $\hat{L}_{heat} = \sqrt{\gamma}\hat{a}^\dagger$, where γ gives the rate of heating. This plot is obtained for a choice of $\gamma = 500\text{s}^{-1}$. The fidelity obtained for this mapping under this choice of parameters is 0.99621, demonstrating the robustness of the MS gate against motional heating.

7 Construction of CNOT

In this final section, we construct the CNOT gate using a combination of the MS gate obtained in Section 3 and single-qubit unitaries. Although the universality criteria for quantum computing

requires only single qubit unitaries and *any* two-qubit entangling unitary (including of course the MS gate), it is still insightful to see explicitly how we can construct CNOT from this gate, as CNOT is more often used in proofs demonstrating universality, and explicitly features in many schematics of various quantum algorithms. Thus, whilst the ability to construct CNOT follows immediately from the property of universality, it is still useful to see *how* this can be constructed, as this provides further insight into the behaviour of the MS gate.

We begin by restating the form of the MS unitary presented at the start of Section 3:

$$U_{MS} = \frac{1}{\sqrt{2}} \begin{pmatrix} 1 & 0 & 0 & -i \\ 0 & 1 & -i & 0 \\ 0 & -i & 1 & 0 \\ -i & 0 & 0 & 1 \end{pmatrix} \tag{71}$$

By inspection, we see that the diagonal basis $\{|\pm\pm\rangle\}$ defined by $|\pm_1\pm_2\rangle \equiv \frac{1}{\sqrt{2}}(|g\rangle\pm_1|e\rangle)\otimes\frac{1}{\sqrt{2}}(|g\rangle\pm_2|e\rangle)$ will diagonalise this unitary. Expressing in this basis, we obtain:

$$U_{MS} = e^{-\frac{i\pi}{4}} \begin{pmatrix} 1 & 0 & 0 & 0 \\ 0 & i & 0 & 0 \\ 0 & 0 & i & 0 \\ 0 & 0 & 0 & 1 \end{pmatrix} \tag{72}$$

Disregarding the global phase, this unitary can be shown to be equivalent to a controlled phase (C-Z) gate up to a global rotation about the z-axis [3].

$$\begin{aligned} \hat{R}_z(-\frac{\pi}{2})U_{MS} &= \begin{pmatrix} 1 & 0 \\ 0 & e^{-\frac{i\pi}{2}} \end{pmatrix} \otimes \begin{pmatrix} 1 & 0 \\ 0 & e^{-\frac{i\pi}{2}} \end{pmatrix} \begin{pmatrix} 1 & 0 & 0 & 0 \\ 0 & i & 0 & 0 \\ 0 & 0 & i & 0 \\ 0 & 0 & 0 & 1 \end{pmatrix} \\ &= \begin{pmatrix} 1 & 0 & 0 & 0 \\ 0 & -i & 0 & 0 \\ 0 & 0 & -i & 0 \\ 0 & 0 & 0 & -1 \end{pmatrix} \begin{pmatrix} 1 & 0 & 0 & 0 \\ 0 & i & 0 & 0 \\ 0 & 0 & i & 0 \\ 0 & 0 & 0 & 1 \end{pmatrix} \\ &= \begin{pmatrix} 1 & 0 & 0 & 0 \\ 0 & 1 & 0 & 0 \\ 0 & 0 & 1 & 0 \\ 0 & 0 & 0 & -1 \end{pmatrix} \\ &= \text{C-Z} \end{aligned} \tag{73}$$

Thus, we obtain a controlled phase gate, defined by the controlled operation of applying $\hat{\sigma}_z$ on the second qubit controlled on the value of the first qubit. To convert this into CNOT, we use the identity $\hat{X} = \hat{H}\hat{Z}\hat{H}$, where $\hat{H}$ is the Hadamard operator [1], to show that CNOT $= (\mathbb{I}\otimes\hat{H})$C-Z$(\mathbb{I}\otimes\hat{H})$:

$$
\begin{aligned}
(\mathbb{I}\otimes\hat{H})\hat{R}_z(-\frac{\pi}{2})U_{MS}(\mathbb{I}\otimes\hat{H}) &= \frac{1}{2}\begin{pmatrix}1&1&0&0\\1&-1&0&0\\0&0&1&1\\0&0&1&-1\end{pmatrix}\begin{pmatrix}1&0&0&0\\0&1&0&0\\0&0&1&0\\0&0&0&-1\end{pmatrix}\begin{pmatrix}1&1&0&0\\1&-1&0&0\\0&0&1&1\\0&0&1&-1\end{pmatrix} \\
&= \begin{pmatrix}1&0&0&0\\0&1&0&0\\0&0&0&1\\0&0&1&0\end{pmatrix} \\
&= \text{CNOT}
\end{aligned} \tag{74}
$$

We note that it is only at this final step when converting from a controlled-phase gate into CNOT that we first require the ability to address a particular qubit in isolation without globally illuminating both ions with the laser. The MS gate itself (as well as its conversion into the controlled-phase gate) involves only global beams, thus eliminating the need to independently focus lasers on individual ions for its execution [3][4], which is a hugely experimentally favourable property of the gate.

8 Bibliography

[1] Nielsen M. and Chuang I. (2010) *Quantum Computation and Quantum Information* Cambridge United Kingdom, Cambridge University Press

[2] Sørensen A. and Mølmer K. (2000) *Entanglement and quantum computation with ions in thermal motion* arXiv:quant-ph/0002024v2 [quant-ph]

[3] Häffner H., Roos C.F. and Blatt R. (2008) *Quantum computing with trapped ions* arXiv:0809.4368 [quant-ph]

[4] Bruzewicz C. D., Chiaverini J., McConnell R. and Sage J. M. (2019) *Trapped-Ion Quantum Computing: Progress and Challenges* arXiv:1904.04178v1 [quant-ph]

[5] Brownnutt M., Kumph M., Rabl P. and Blatt R. (2014) *Ion-trap measurements of electric-field noise near surfaces* arXiv:1409.6572v1 [quant-ph]

[6] Roos C.F. (2008) *Ion trap quantum gates with amplitude-modulated laser beams* New J. Phys. 10 013002

[7] Kirchmair G., Benhelm J., Zäringer F., Gerritsma R., Roos C.F. and Blatt R. (2009) *Deterministic entanglement of ions in thermal states of motion* arXiv:0810.0670 [quant-ph]

[8] Blanes S., Casas F., Oteo J.A. and Ros J. (2008) *The Magnus expansion and some of its applications* arXiv:0810.5488v1 [math-ph]

[9] Grynberg G., Aspect A. and Fabre C. (2010) *Introduction to Quantum Optics* Cambridge United Kingdom, Cambridge University Press

[10] Schäfer V.M., Ballance C.J., Thirumalai K., Stephenson L.J., Ballance T.G., Steane A.M. and Lucas D.M. (2018) *Fast quantum logic gates with trapped-ion qubits* arXiv:1709.06952v2 [quant-ph]

[11] Schindler P. *et al* (2013) *A quantum information processor with trapped ions* New J. Phys. 15 123012

[12] Preskill J. (1998) *Lecture Notes for Physics 229: Quantum Information and Computation* California Institute of Technology

Appendix

A.1 Deriving the von Neumann equation in the Interaction Picture

The von Neumann equation for the time-evolution of some density operator ρ under some Hamiltonian H is given by:

$$\frac{d}{dt}\rho = -\frac{i}{\hbar}[H, \rho] \tag{75}$$

For $H = H_0 + H_{int}$, where H_0 gives the unperturbed core Hamiltonian of the system and H_{int} describes interactions with the environment, it is common to transform into a frame rotating with H_0 to simplify the problem. This frame is sometimes called the *interaction picture*, and taking H_0 to be time-independent, transformations into it can be achieved through the mappings:

$$\begin{aligned} \rho \to \tilde{\rho} &\equiv \exp(\frac{iH_0t}{\hbar})\ \rho\ \exp(\frac{-iH_0t}{\hbar}) \\ H_{int} \to \tilde{H}_{int} &\equiv \exp(\frac{iH_0t}{\hbar})\ H_{int}\ \exp(\frac{-iH_0t}{\hbar}) \end{aligned} \tag{76}$$

In the following we will derive the resulting dynamical equation for time-evolution of $\tilde{\rho}$. After solving this equation, we can then obtain time-evolution of the original density matrix ρ by simple reversal of the unitary transformation given in (76). The motivation for this whole procedure is that it is typically much easier to work in the interaction picture than to directly solve (75) with the full Hamiltonian H. This is because we will find that in the interaction picture, the phase evolution of eigenstates of H_0 will become absorbed into the definitions of $\tilde{H}_{int}$ and $\tilde{\rho}$ such that explicit dependence on H_0 disappears.

$$\begin{aligned} \frac{d}{dt}\tilde{\rho} &= \frac{d}{dt}(\exp(\frac{iH_0t}{\hbar})\ \rho\ \exp(\frac{-iH_0t}{\hbar})) \\ &= \frac{iH_0}{\hbar}\tilde{\rho} + e^{\frac{iH_0t}{\hbar}}(\frac{d}{dt}\rho)e^{-\frac{iH_0t}{\hbar}} - \tilde{\rho}\frac{iH_0}{\hbar} \\ &= \frac{i}{\hbar}[H_0, \tilde{\rho}] + e^{\frac{iH_0t}{\hbar}}(-\frac{i}{\hbar}[H, \rho])e^{-\frac{iH_0t}{\hbar}} \quad \text{(from (75))} \\ &= \frac{i}{\hbar}[H_0, \tilde{\rho}] + e^{\frac{iH_0t}{\hbar}}(-\frac{i}{\hbar}[H_0 + H_{int}, \rho])e^{-\frac{iH_0t}{\hbar}} \\ &= \frac{i}{\hbar}[H_0, \tilde{\rho}] - \frac{i}{\hbar}[H_0, \tilde{\rho}] - \frac{i}{\hbar}e^{\frac{iH_0t}{\hbar}}[H_{int}, \rho]e^{-\frac{iH_0t}{\hbar}} \quad \text{(as } [H_0, H_0] = 0) \\ &= -\frac{i}{\hbar}[\tilde{H}_{int}, \tilde{\rho}] \end{aligned} \tag{77}$$